

This is the preprint version of the contribution published as:

Rabot, E., Wiesmeier, M., Schlüter, S., Vogel, H.-J. (2018):
Soil structure as an indicator of soil functions: A review
Geoderma **314** , 122 – 137

The publisher's version is available at:

<http://dx.doi.org/10.1016/j.geoderma.2017.11.009>

1 **Soil structure as an indicator of soil functions: a review**

2 **E. Rabot^a, M. Wiesmeier^b, S. Schlüter^a, H.-J. Vogel^{a,*}**

3 ^a Helmholtz Centre for Environmental Research – UFZ, Department of Soil Physics, Halle
4 (Saale), Germany

5 ^b Chair of Soil Science, TUM School of Life Sciences Weihenstephan, Technical University
6 of Munich, Freising, Germany

7 * Corresponding author: hans-joerg.vogel@ufz.de (H.-J. Vogel)

8 **Abstract**

9 Since many processes in soil are highly sensitive to soil structure, this review intends to
10 evaluate the potential of observable soil structural attributes to be used in the assessment of
11 soil functions. We focus on the biomass production, storage and filtering of water, storage and
12 recycling of nutrients, carbon storage, habitat for biological activity, and physical stability and
13 support. A selection of frequently used soil structural properties are analyzed and discussed
14 from a methodological point of view and with respect to their relevance to soil functions.
15 These are properties extracted from soil profile description, visual soil assessment, aggregate
16 size and stability analysis, bulk density, mercury porosimetry, water retention curve, gas
17 adsorption, and imaging techniques. We highlight the greater relevance of the pore network
18 characterization as compared to the aggregate perspective. We identify porosity,
19 macroporosity, pore distances and pore connectivity derived from imaging techniques as
20 being the most relevant indicators for several soil functions. Since imaging techniques are not
21 widely accessible, we suggest using this technique to build up an open access “soil structure
22 library” for a large range of soil types, which could form the basis to relate more easily
23 available measures to pore structural attributes in a site-specific way (i.e., taking into account
24 texture, soil organic matter content, etc.).

25 **Keywords:** Soil structure, soil functions, Visual soil assessment; Aggregate size distribution
26 and stability; Bulk density; Mercury porosimetry; Water retention curve; Imaging techniques

27 **Abbreviations:** BD, bulk density; DC, degree of compactness; LLWR: least limiting water
28 range; MIP: mercury intrusion porosimetry; SOM, soil organic matter

29 **1. Introduction**

30 Soil structure is recognized to control many processes in soils. It regulates water retention and
31 infiltration, gaseous exchanges, soil organic matter and nutrient dynamics, root penetration,
32 and susceptibility to erosion. Soil structure also constitutes the habitat for a myriad of soil
33 organisms, consequently driving their diversity and regulating their activity (Elliott and
34 Coleman, 1988). As an important feedback, soil structure is actively shaped by these
35 organisms, thus modifying the distribution of water and air in their habitats (Bottinelli et al.,
36 2015; Feeney et al., 2006; Young et al., 2008). Since many processes in soil proved to be
37 linked to soil structure, this review intends to evaluate the potential of soil structure to be used
38 in the assessment of soil functions. We refer to soil structure as the spatial arrangement of
39 solids and voids across different scales without considering the chemical heterogeneity of the
40 solid phase. Thus, the solid phase and pore space are complementary aspects of soil structure
41 which can be approached from both perspectives.

42 The solid phase perspective, based on mechanisms of soil aggregation, has been supported by
43 Tisdall and Oades (1982). Since their pioneering work, aggregation is conceptually viewed as
44 a three-stage hierarchical organization of the soil solid phase, each stage involving
45 characteristic binding agents. Primary particles ($< 20 \mu\text{m}$) are bound together into
46 microaggregates ($20\text{--}250 \mu\text{m}$), which are bound together to form macroaggregates
47 ($> 250 \mu\text{m}$). Follow-up studies favored a different sequence of aggregate formation:
48 macroaggregates can form around particulate organic matter, then microaggregates are

49 released upon breakdown of macroaggregates (Angers et al., 1997; Oades, 1984). The bonds
50 within microaggregates are supposed to be more persistent than those between
51 macroaggregates (Tisdall and Oades, 1982). This hierarchical order, responsible for the
52 micro- and macroaggregate formation, was identified in soils where soil organic matter was
53 the major binding agent, but could neither be found in oxide-rich nor in sandy soils
54 (Christensen, 2001; Oades and Waters, 1991; Six et al., 2004).

55 Following a pore perspective, soil structure may not be defined as “the shape, size and spatial
56 arrangement of primary soil particles and aggregates” but as “the combination of different
57 types of pores” (Pagliai and Vignozzi, 2002), where the existence of aggregates is not
58 required and soil particle surfaces are assumed to be the walls of the pore space (Elliott and
59 Coleman, 1988). Similar to the aggregate hierarchy, a hierarchy of pores can be defined
60 (Elliott and Coleman, 1988). Depending on their size, pores are classified as macropores,
61 mesopores, and micropores, although there are no generally agreed upon size thresholds
62 between these categories. Pores resulting from the arrangement of soil primary particles are
63 called textural pores, whereas bigger pores resulting from biotic factors, climate, and
64 management practices are called structural pores.

65 These two different perspectives rely on the perception of what is actively shaped: aggregates
66 or pores. Considering the multitude of soil processes and their interactions, there is ample
67 evidence that generally both are possible with changing balance depending on soil type and
68 site conditions. Irrespective of these different perspectives, there are distinct methods
69 available to characterize either the solid phase arrangement or the pore space, and the
70 obtained results are expected to differ in sensitivity, cost, or relevance to soil functions.

71 Yet, there is no universally accepted way to characterize soil structure (Díaz-Zorita et al.,
72 2002), and this is even more true for using soil structural measures as indicators for soil
73 functions as we intend to do. Wallace (2007) describes ecosystem functions as a synonym of

74 ecosystem processes. Therefore, soil functions refer to “what the soil does” (Seybold et al.,
75 1998), i.e., intrinsic processes occurring in soils irrespective of any human interest. From this
76 definition, we assume that it is possible to assess soil functions through information-bearing
77 soil properties called indicators. Good indicators must be highly correlated with the function
78 of interest (Reinhart et al., 2015), that is to say, with other soil properties governing soil
79 processes (e.g., saturated hydraulic conductivity, air permeability, etc.). They must also be
80 sensitive enough to detect changes in soil conditions resulting from different management
81 practices and land uses. Their measurement must be reliable and reproducible. The monetary
82 and human costs for their acquisition and the level of expertise needed are also important
83 aspects. A wide number of methods and structural properties are currently used by soil
84 scientists and farmers, from quick field observations to thorough laboratory characterizations.
85 Our intention is to provide a critical analysis of their efficiencies as related to soil functions.

86 We will particularly focus on six soil functions: biomass production, storage and filtering of
87 water, storage and recycling of nutrients, carbon storage, habitat for biological activity, and
88 physical stability and support. Attention will be paid on structural soil properties
89 representative at the scale of pedons and soil horizons, assuming that soil functions can be
90 assessed for 1-D soil profiles in a meaningful way. Since it is essential that the methods used
91 be reliable from a technical point of view, we will discuss corresponding advantages and
92 limitations. We will also report to what extent simple methods can substitute more complex
93 ones to find a trade-off between reliability of information and acquisition cost. We will
94 evaluate the different methods in terms of sampling requirements, reproducibility, cost, and
95 level of expertise required. We chose to separate the available approaches to characterize soil
96 structure based on the solid phase arrangement from those based on the pore space
97 perspective.

98 **2. Characterization of the solid phase arrangement**

99 **2.1. Field methods**

100 Methods available to characterize soil structure directly in the field mainly aim at describing
101 the “macrostructure”, that is to say, visible to the naked eye (Baize et al., 2013). They can
102 roughly be divided in two groups: the whole profile evaluation, developed from the
103 fundamental methods of field surveys, and the topsoil evaluation, a simplified version
104 especially designed for farmers.

105 **2.1.1. Whole profile evaluations**

106 Following the FAO (2006) guidelines and most of the national standards (e.g., Ad-hoc-AG
107 Boden, 2005 in Germany; Baize and Jabiol, 2011 in France; Schoeneberger et al., 2012 in the
108 USA), soil structure morphology and its variation with depth are evaluated visually as part of
109 the soil profile description. The description of soil structure is mainly related to its grade, and
110 the size and shape of aggregates (Ad-hoc-AG Boden, 2005; Baize and Jabiol, 2011; FAO,
111 2006; Schoeneberger et al., 2012). The term aggregates usually comprises peds, fragments,
112 and clods. Aggregates formed by natural processes are called peds, small aggregates formed
113 artificially during laboratory or field manipulations are called fragments, and large aggregates
114 formed artificially by cultivation operations are called clods. When soil material breaks into
115 aggregates of higher order than the single grains (pedal soils), structure can be addressed by
116 describing the grade of these aggregates. The grade describes the distinctness of the
117 aggregates in place, qualified as strong, moderate, or weak. Qualifying the grade is realized
118 by observing whether soil material breaks into fragments or “powder” when disturbed, and to
119 what extent the surface of aggregates differs from their inner part (FAO, 2006). The aggregate
120 shape is described according to several types of soil structure: among others, angular blocky,
121 subangular blocky, granular, platy, prismatic, or columnar. In structureless soils (apedal

122 soils), no aggregate are observed and the material is either compact or built up by single
123 grains. The size, abundance, orientation, and continuity of voids can also be described in the
124 field, with the naked eye or a hand-lens. As suggested in the FAO (2006) guidelines, the
125 description of voids emphasizes continuous and elongated voids, i.e., animal burrows, root
126 channels, or cracks. However, the description of the complete void organization cannot be
127 done (Baize and Jabiol, 2011).

128 Field observations of aggregate size, shape, and grade are rarely used as indicators for soil
129 functions. Pulido Moncada et al. (2014c) used aggregate shape (FAO, 2006) assuming that
130 rounded aggregates are of “good” quality for crop growth compared to soils with angular
131 aggregates,. This simplified indicator was sensitive to soil type for the two studied soils, but
132 appeared to be poorly sensitive to land use (in this study, cereal monoculture vs. permanent
133 pasture). By applying regression trees on a database gathering water retention measurements
134 and field descriptions of soil structure, Pachepski and Rawls (2003) found that the grade of
135 soil structure, classified as strong, moderate, or weak, was the most informative to explain the
136 water retention values, followed by the aggregates size and shape. In this case, water retention
137 was correlated with the grade, because of the water capacity of small intra-aggregate pores.
138 However, the overall discriminating power of the aggregate grade, size, and shape depended
139 on the texture class.

140 Another whole profile evaluation method is called “*profil cultural*” method, initially
141 developed for tilled layers (Roger-Estrade et al., 2004) and recently for no-till soils (Boizard
142 et al., 2017). This method is usually applied to the soil profile down to approximately 1 m
143 depth. A map of the vertical face of a pit is produced, showing different types of clods
144 distinguished according to the visual inspection of their internal porosity: Γ clods (with high
145 visible porosity), Δ clods (without visible porosity), and Φ clods (with cracks due to
146 weathering). Contours are drawn manually on a photograph of the soil profile to quantify clod

147 surfaces (Figure 1). Roger-Estrade et al., (2000) used the percentage of severely compacted
148 zones showing no visible porosity (Δ clods) as an indicator of soil structure, They found that
149 the temporal dynamics of this indicator was different from that of soil bulk density (BD) as
150 measured with a gamma-ray probe, because the gamma-ray probe averaged highly
151 fragmented and highly compacted zones. Lower void ratio, lower soil deformability, and
152 higher precompression stress were found for Δ clods, as compared to the more porous Γ clods,
153 thus validating this visual classification (Roger-Estrade et al., 2004).

154 The description of soil structure in the field highly depends on soil moisture, especially in
155 swell-shrinking soils. Therefore, the FAO (2006) guidelines recommend performing this
156 description when the soil is dry or slightly moist. The whole profile evaluations provide
157 valuable information on the vertical sequence of soil structural properties. However, they are
158 subjective, and since they require the digging of pits, they are also time consuming, and
159 sufficient replication cannot always be done (Mueller et al., 2009).

160 2.1.2. Topsoil evaluation

161 Because accurate soil profile description requires considerable experience, simplified
162 approaches based on field tests were designed to assess physical properties visually
163 (Shepherd, 2000). They are particularly developed to estimate soil quality and are highly
164 relevant for farmers or land managers, who wish to evaluate the quality of their soils and their
165 management practices, easily, quickly, and cheaply. Indeed, the evaluation is often performed
166 in less than 20 minutes, with a spade being the main required equipment. Several “spade
167 tests” were proposed, such as the Peerlkamp (1959) test, the “Visual Evaluation of Soil
168 Structure” (Ball et al., 2007; Guimarães et al., 2011), the “Visual Soil Assessment”
169 (Shepherd, 2009, 2000), or the “SOILpak score” (McKenzie, 2001). A similar approach exists
170 for subsoil (Ball et al., 2015). In the topsoil evaluations, an undisturbed soil block is extracted
171 from soil surface with a spade (e.g., full size of the spade and approximately 20 cm-thick) and

172 manually broken or dropped from a 1 m-height to produce aggregates. Aggregates are then
173 described in terms of size, porosity, shape, color, ease of breakup, together with the
174 identification of the presence of a tillage pan, depth of root penetration, or the number of
175 earthworms. The soil samples are then compared to the photographs of a reference key to
176 score soil structure (Figure 2). ~~To ensure a representative scoring, several soil samples are~~
177 ~~generally evaluated at a given site, e.g., 3 to 4 in Shepherd (2000), 10 in Guimarães et al.~~
178 ~~(2011), or 10 to 20 in Ball et al. (2007). Shepherd (2000) recommends to also evaluate a soil~~
179 ~~unaffected by management practices to allow for comparisons.~~

180 These visual soil evaluation methods usually demonstrated a good sensitivity to different
181 management practices (Ball et al., 2007; Giarola et al., 2013; Guimarães et al., 2011), and
182 were particularly useful to detect soil compaction. Scores were correlated to the agricultural
183 productivity function (Mueller et al., 2009), to water infiltration through the saturated
184 hydraulic conductivity (Mueller et al., 2009; Pulido Moncada et al., 2014b; Shepherd, 2003),
185 and to gas transport through the air permeability and air capacity (Guimarães et al., 2013;
186 Shepherd, 2003). A “good” soil structure, according to the visual soil evaluation scores, was
187 associated with a low soil BD, low penetration resistance, low tensile strength, low
188 compaction state as estimated with the degree of compactness, or high number of pore
189 branches (Garbout et al., 2013; Guimarães et al., 2013, 2011; Mueller et al., 2009; Newell-
190 Price et al., 2013; Pulido Moncada et al., 2014b).

191 The main drawback of visual soil evaluation methods is the considerable subjectivity
192 introduced, for example, by the scoring with a reference to photographs. In addition, when the
193 method requires to break the soil manually to produce aggregates (e.g., Ball et al., 2007), the
194 results depend on the experience of the operator (Giarola et al., 2013; Guimarães et al., 2011).
195 In order to standardize this procedure, Shepherd (2009, 2000) rather uses the drop-shatter test,
196 where the soil block is dropped from a 1 m-height on a wooden board, a maximum of three

197 times. However, as with other methods to identify aggregates, the results are sensitive to the
198 actual water content (Guimarães et al. 2011). In addition, with the drop-shatter test a mixture
199 of the entire spade length is analyzed. When clods are broken manually, the final score is
200 calculated as the weighted mean of each layer score, with layer thicknesses as weights (e.g.,
201 Ball et al., 2007). This reduces the efficiency of the visual soil evaluation score as an indicator
202 of soil function when contrasting layers, potentially limiting for some soil functions, are
203 present (Newell-Price et al., 2013; Pulido Moncada et al., 2014c). Although the different
204 visual soil evaluation methods gave similar trends when comparing different sites, they can
205 lead to very different classes of soil physical quality (Giarola et al., 2013; Mueller et al., 2009;
206 Newell-Price et al., 2013).

207 It has been recognized that the results of such visual evaluations are sensitive to soil texture
208 (Giarola et al., 2013; Newell-Price et al., 2013) since coarser, less cohesive soils break up into
209 finer fragments and getting higher scores. Moreover, the results depend on soil water content
210 (Guimarães et al., 2011) and on biological activity and herewith on the growing season
211 (Mueller et al., 2009). Yet, the range of water content at which the evaluation is performed is
212 not standardized (Guimarães et al., 2017).

213 In summary, methods of visual inspection remain poorly used in research, because they are
214 operator dependent and only provide semi-quantitative results. Also, a dedicated training is
215 required before application. Moreover, the sensitivity of the simple visual criteria to changes
216 in management practices could be weak (Nortcliff, 2002; Pulido Moncada et al., 2014a) and if
217 a decline in soil structure is recorded via visual assessment, it could be already too late to
218 adapt the management practices (Nortcliff, 2002).

219 **2.2. Laboratory methods**

220 In this section, we review structural soil properties obtained for soil samples collected in the
221 field, then analyzed with more or less labor-intensive methods in the laboratory to
222 characterize the solid phase arrangement.

223 2.2.1. Bulk density and derived indicators

224 One of the most prominent indicators of soil structure is soil bulk density (or dry bulk
225 density), because it does not require any specific expertise or expensive equipment. It is
226 calculated as the ratio of the dry mass of solids to the undisturbed soil volume . Porosity can
227 then be derived from BD, knowing or approximating the particle density value. Samples of
228 known volume are typically obtained by using cores (or volumetric ring) of a well-defined
229 size. Alternatives are the excavation, or the clod method which are more labor-intensive, since
230 the sampled volume is not known a priori and needs to be determined after extraction. In the
231 excavation method, the volume is estimated by measuring the elevation of the ground surface
232 before and after excavation (Soil Survey Staff, 2014), or by filling the hole left with water,
233 sand, or another material like expanding polyurethane foam (Laundré, 1989) or plaster
234 (Frisbie et al., 2014). The excavation method is particularly adapted for loose soils, where a
235 coherent sample cannot be collected (Harrison et al., 2003). In the clod method, the clod is
236 first coated or saturated with a water repellent substance (e.g., paraffin) to prevent water from
237 entering the clod, and the volume is then determined by water displacement. This method can
238 also be used to measure the aggregate density (e.g., Rücknagel et al., 2007). Other variants of
239 volume determination exist, such as photogrammetric method (Bauer et al., 2014), 3-D laser
240 scanning (Rossi et al., 2008), or the use of a pycnometer (Uteau et al., 2013). It is worth
241 noting that some sensors were developed to estimate BD directly in the field to collect high
242 amounts of data in a shorter period of time, such as the gamma radiation transmission or
243 scattering methods (Holmes et al., 2011; Page-Dumroese et al., 1999; Timm et al., 2005) or

244 the thermo-time domain reflectometry (Lu et al., 2016). The soil water content and sometimes
245 the particle size distribution need to be known to relate the sensor response to BD.

246 The various methods are prone to some errors in BD determination (Page-Dumroese et al.,
247 1999). By definition, the clod method gives an inadequate representation of large pores, since
248 inter-clod pores are not sampled. When collecting replicates in a given area, the calculated
249 standard deviations are thus low, because the variability linked with large pores is removed
250 (Timm et al., 2005). With the core method, soil compaction may occur during sampling
251 (Håkansson, 1990; Page-Dumroese et al., 1999; Schlüter et al., 2011). Moreover, with small-
252 diameter cores, the standard deviations tend to be high in case the representative elementary
253 volume with respect to soil structure is larger (Page-Dumroese et al., 1999; Timm et al.,
254 2005). Obtaining reliable BD measurements in soils with abundant rock fragments is
255 recognized to be even more challenging. Indeed, rocks can obstruct ring penetration and rock
256 fragments larger than the cylinder diameter are excluded (Harrison et al., 2003; Page-
257 Dumroese et al., 1999; Throop et al., 2012; Vincent and Chadwick, 1994), so that the fine –
258 textured soil tends to be over-represented (Harrison et al., 2003). Moreover, the representative
259 elementary volumes are very large (Vincent and Chadwick, 1994). The excavation method is
260 probably more efficient in this case (Harrison et al., 2003; Page-Dumroese et al., 1999).
261 Similar problems arise in vegetated soils, where the presence of plant roots or residues tends
262 to guide the sampling in a subjective way. For swell-shrinking soils, the volume depends on
263 the water content during sampling, which should be well defined to get comparable results
264 (Keller and Håkansson, 2010; Mueller et al., 2009). Moebius et al. (2007) recommend
265 measuring BD during spring time when soils are close to field capacity to reduce the
266 variability linked to the soil water content.

267 BD is mainly considered to be useful to estimate soil compaction. Root length density, root
268 diameter, and root mass were observed to decrease after an increase in BD (Dal Ferro et al.,

269 2014). However, the interpretation of BD with respect to soil functions depends on soil type,
270 especially soil texture and soil organic matter (SOM) content. Moreover, no strong link with
271 the crop production function has been found, because the optimal BD for crop growth
272 depends on soil texture and plant physiology (Kaufmann et al., 2010).

273 Some authors suggested using the degree of compactness (DC, also called relative BD) as a
274 less site-specific, and therefore more powerful indicator of the compaction state of ploughed
275 layers (e.g., da Silva et al., 1997; Håkansson, 1990; Håkansson and Lipiec, 2000). To remove
276 the effect of soil type, DC is defined as the ratio of soil BD to the reference BD_{ref} of the same
277 soil, which is thought to represent the maximum compression state that the soil can
278 experience in field conditions. To measure BD_{ref} , uniaxial compression tests (e.g., da Silva et
279 al., 1997; Håkansson, 1990) or Proctor tests (e.g., de Oliveira et al., 2016) were used at
280 various loads or energy levels. Yet, there is no standard procedure so that different values for
281 BD_{ref} and DC are obtained (Håkansson, 1990; Naderi-Boldaji and Keller, 2016; Reichert et
282 al., 2009). The normalization aims at removing the dependency of BD to clay and SOM
283 content. It proved to be efficient under soils derived from similar parent materials and climatic
284 conditions (da Silva et al., 1997). However, it was not satisfying for organic soils (Håkansson,
285 1990). A negative linear relationship was found between DC and macroporosity, and between
286 DC and the logarithm of saturated hydraulic conductivity (Reichert et al., 2009). With respect
287 to plant growth, an optimum function was defined by Reichert et al. (2009), who found the
288 highest yields for DC values between 80 and 90%, but with considerable uncertainty due to
289 the considered crop and the method used to define BD_{ref} (Reichert et al., 2009).

290 The packing density is another indicator derived from BD describing the state of compaction
291 (Renger, 1970). A correction term is added to BD to account for the clay content in estimating
292 the critical compaction with respect to crop growth. The correction term is defined as the
293 product of the clay content and the slope of the regression between BD and clay content

294 (Renger, 1970). A correction for the silt dependency can also be applied (Renger et al., 2008).
295 In this way, it becomes possible to define a unique threshold of packing density to
296 characterize optimal crop growth, valid for a variety of soil types. A packing density
297 $< 1.7 \text{ g cm}^{-3}$ would be optimal for crop growth and limiting for crop growth when
298 $> 1.7 \text{ g cm}^{-3}$ (Kaufmann et al., 2010). This parameter has been poorly explored so far.

299 2.2.2. Aggregate size distribution and stability

300 Another common way to characterize the solid phase arrangement and its supposed
301 hierarchical orders is through the analysis of the aggregate-size distribution and aggregate
302 stability, i.e., the ability of soil to retain its structure under the actions of water and
303 mechanical stress (Dexter, 1988). In the laboratory, the aggregate size can be characterized
304 more thoroughly than in the field (section 2.1.1). Aggregates are broken to a number of size
305 fractions following various protocols (Díaz-Zorita et al., 2002). During “dry sieving”, air- or
306 oven-dried soil samples are sieved for a given duration or until complete separation. For “wet
307 sieving”, dried, field moist, or rewetted soil samples are immersed in water, and in some
308 cases, submitted to oscillating sieves. Some other protocols use a rainfall simulator (e.g.,
309 Almajmaie et al., 2017; Moebius et al., 2007). During wet sieving, aggregates are subjected to
310 slaking due to fast wetting of dry aggregates, micro-cracking through differential swelling, or
311 mechanical breakdown (Le Bissonnais, 1996). The proportion of fragments $> 250 \mu\text{m}$
312 constitutes the water-stable aggregates, whereas the $50\text{--}250 \mu\text{m}$ fraction represents the water-
313 stable microaggregates (Dexter, 1988). Some other solvents can be used, such as ethanol or
314 benzene, in order to modify the wetting properties (Le Bissonnais, 1996). Microaggregate
315 stability is also studied by measuring the water-dispersible clay fraction (Brubaker et al.,
316 1992; Calero et al., 2008; Czyż and Dexter, 2015; Paradelo et al., 2013).

317 Then, indices are computed to express the results (Díaz-Zorita et al. 2002). Aggregate size
318 distribution is characterized after fitting a distribution functions to obtain the mean and

319 standard deviation for a Gaussian, or the geometric mean diameter for a log-normal
320 distribution. Aggregate stability is characterized by analyzing the stable aggregate size before
321 and after some energy input. Other indices are directly computed based on a single aggregate
322 size class, to allow for comparisons between soils of various structures (Le Bissonnais, 1996).
323 Water-dispersible clay can be directly used as an indicator but can also be combined with
324 water-dispersible silt, and total clay and silt contents, as suggested by Igwe and Udegbunam
325 (2008).

326 The main drawback of using aggregate size distribution and stability as indicators is that the
327 results are highly sensitive to methodological details as the type of sieving, its duration,
328 oscillation frequency and loading rate (Almajmaie et al., 2017; Beare and Bruce, 1993; Letey,
329 1991) and a large number of different methods are actually used (Díaz-Zorita et al., 2002; Le
330 Bissonnais, 1996; Peng et al., 2015).. There is, however, a protocol developed by Le
331 Bissonnais (1996) for assessing the stability of soil aggregates subjected to the action of water
332 by combining three tests, which led to an international standard (ISO 10930, 2012). Other
333 important aspects are the sample pretreatments aiming at homogenizing the water contents
334 (e.g., air-dried samples or rewetted at a given water potential), since they modify the bonding
335 forces (Almajmaie et al., 2017; Beare and Bruce, 1993; Haynes, 1993). Similar to aggregate
336 stability tests, water-dispersible clay measurement proved to be highly sensitive to
337 pretreatments (i.e., initial water content and wetting rate) and to the amount of energy applied
338 for the dispersion (Czyż and Dexter, 2015; Kjaergaard et al., 2004). So, the results of the
339 different dry and wet sieving protocols were not always consistent, and their ability to
340 discriminate management practices, soil properties, or measured soil loss varied greatly (Le
341 Bissonnais, 1996; Pulido Moncada et al., 2013). Another aspect is that the mechanical work
342 applied during dry sieving is rarely experienced in the field and cannot be easily quantified

343 (Díaz-Zorita et al., 2002). In the same way, the positive pore water pressures applied during
344 wet sieving rarely occur under natural conditions.

345 Significant positive correlations between the aggregate size and macroporosity, number of
346 pores, and pore size were observed (Mangalassery et al., 2013). According to Dexter (1988),
347 there is an optimal aggregate size for seed germination between 1 and 5 mm in diameter
348 (physical support function). Aggregate size was also observed to influence the emissions of
349 CO₂, N₂O, and CH₄ (Drury et al., 2004; Mangalassery et al., 2013). However, the existence
350 and direction of the relationships depended on soil texture and SOM content (Mangalassery et
351 al., 2013). Soil aggregation further regulates the capacity of soils to store carbon by physical
352 protection of SOM from microbial and enzymatic attack. The protective capacity of
353 aggregates is mainly related to a spatial separation of substrate and microorganisms as well as
354 to a reduced microbial activity due to a reduced diffusion of oxygen into aggregates (Six et
355 al., 2002). Evidence was found that stable microaggregates play a decisive role for the long-
356 term stabilization of SOM, whereas less stable macroaggregates provide only a minimum of
357 physical protection (Krull et al., 2003; Six et al., 2004, 2002). In this regard, silt-sized
358 microaggregates seem to be of particular importance for carbon storage in both topsoils and
359 subsoils (Han et al., 2015; Moni et al., 2010; Virto et al., 2008). As a measureable indicator,
360 microaggregates-within-macroaggregates were proposed as diagnostic fraction for the carbon
361 sequestration potential in agroecosystems and for soil organic carbon changes induced by
362 management and land use changes in a wide range of soil types and environments (Denef et
363 al., 2007, 2004; Kong et al., 2005; Six and Paustian, 2014).

364 Aggregate stability was found to be significant for the susceptibility to erosion of soils
365 (Nciizah and Wakindiki, 2015). Many authors reported that reduced aggregate stability
366 increases soil susceptibility to runoff, interrill erosion, and crusting (Barthès and Roose, 2002;
367 Nciizah and Wakindiki, 2015). Crusting is often associated with a reduction of soil aeration

368 and soil permeability. Therefore, aggregate stability and water-dispersible clay are related to
369 the physical stability and support for plants and to the partitioning of water between
370 infiltration and runoff. In addition, since the clay fraction can transport adsorbed nutrients or
371 contaminants along the soil surface with runoff, or downward in the soil profile with
372 infiltrating water (Calero et al., 2008; Czyż and Dexter, 2015), there is a link between
373 aggregate stability and the functions of soils for nutrient cycling and for filtering water.

374 **3. Characterization of the pore space**

375 Some laboratory and imaging techniques were designed to characterize the pore space. Given
376 the typical sample sizes of centimeters to decimeters (Figure 3), these methods mainly
377 characterize the “microstructure” (Baize et al., 2013).

378 **3.1. Indirect methods**

379 Indirect methods use probe molecules to derive information about the pore size, volume,
380 and/or pore-solid surface area. As opposed to imaging techniques, these methods are not
381 spatially resolved and do not characterize the morphology and topology of the pore space.

382 **3.1.1. Mercury porosimetry**

383 Mercury porosimetry is a routine method used for decades for the characterization of the pore
384 size distribution. The main reason for its wide use probably lies in the large range of pore
385 sizes that can be investigated in a single run: usually five orders of magnitude, from about
386 3 nm to 500 μm . A mercury porosimetry analysis is completed within a few hours on soil
387 aggregates between about 2 to 6 cm^3 in size. Instruments are easily available and the
388 repeatability of the method is good. According to Giesche (2006), the standard deviations of
389 pore size and pore volume are < 1%.

390 Usually, mercury porosimetry is performed in its “intrusion” mode (MIP). As a non-wetting
391 fluid, mercury is forced to intrude a soil sample by applying known increasing pressures, to
392 fill pores of decreasing sizes (Van Brakel et al., 1981). Finally, the volume of intruded
393 mercury as function of the applied pressure is obtained. Pressures are converted into
394 equivalent pore diameters according to the Young-Laplace law, assuming non-connected
395 cylindrical pores, to retrieve the pore size distribution. This equation gives the equivalent pore
396 diameter as function of the pressure, contact angle, and surface tension of mercury. Although
397 rarely done in soil science, mercury porosimetry can also be performed in the “extrusion”
398 mode, by decreasing the applied pressure (e.g., Jozefaciuk et al., 2015; Otalvaro et al., 2016).
399 A hysteresis is typically found between intrusion and extrusion: mercury can be entrapped in
400 the soil pore space, because of the ink-bottle effect and different contact angles between
401 advancing and receding menisci (Kloubek, 1981). Jozefaciuk et al. (2015) found, for example,
402 differences from 2.4 to 3.5% in pore volume at equivalent capillary pressures between the
403 intrusion and extrusion curves.

404 MIP often allows distinguishing structural and textural pores, the latter being divided between
405 lacunar and clay fabric pores (Fiès, 1984). To simplify comparisons between samples, pore
406 sizes can also be classified as cryptopores ($< 0.1 \mu\text{m}$), ultramicropores ($0.1\text{--}5 \mu\text{m}$),
407 micropores ($5\text{--}30 \mu\text{m}$), mesopores ($30\text{--}75 \mu\text{m}$), and macropores ($> 75 \mu\text{m}$) (Cameron and
408 Buchan, 2006).

409 Several drawbacks are known to affect MIP, impeding a clear interpretation of the results
410 (Van Brakel et al., 1981). Indeed, in the case of an “ink-bottle” pore, MIP does not measure
411 the actual pore size, but the largest entrance pressure towards this pore, i.e., the neck, and then
412 assumes cylindrical pores when applying the Young-Laplace law to convert pressures into
413 pore diameters (Giesche, 2006). Therefore, pore sizes measured by MIP are always smaller
414 than those measured by imaging methods (Bruand and Cousin, 1995; Giesche, 2006). Even

415 though this is a well-known effect, it is often omitted when interpreting MIP data, assuming
416 that all the compared samples are affected in the same manner. Only a few studies really
417 discussed their results taking into account the ink-bottle effect: for example, in Bruand and
418 Cousin (1995) and Richard et al. (2001), the partial distortion of structural pores during soil
419 compaction created necks, only accessible at high pressure of mercury, classifying them as
420 textural pores instead of structural pores. For this reason, studying compaction with MIP
421 requires special care. In addition, MIP cannot give information on pores disconnected from
422 the external surface of the investigated aggregate. The derived total porosity is thus
423 underestimated. Another source of error lies in the assumptions of a fixed contact angle,
424 usually 130 or 140°. However, the contact angle is supposed to vary depending on surface
425 roughness, pore geometry, mineralogy, and whether the meniscus is advancing or receding
426 (Kloubek, 1981).

427 Soil samples need to be first dried otherwise the remaining water would impede mercury
428 intrusion. This drying step is critical for materials with swelling and shrinking properties due
429 to changes in pore geometry and particle rearrangement. Air-drying (Pagliai et al., 2004),
430 oven-drying at 105°C (Bruand and Cousin, 1995; Diamond, 1970) with a possible preliminary
431 step in a desiccator (Paz Ferreiro et al., 2010), freeze-drying (Cuisinier and Laloui, 2004;
432 Delage and Pellerin, 1984), or acetone vapor exchange (Thompson et al., 1985) were used for
433 example. When compared, these drying techniques led to different porosities and pore size
434 distributions (Cuisinier and Laloui, 2004; Thompson et al., 1985), so none of them can be
435 considered as a standard. Moreover, there are dissenting opinions regarding the possible
436 modification of soil structure during the process of mercury intrusion (Kozak et al., 1991;
437 Lawrence, 1978), which appeared to be more critical for organic soils (Echeverría et al.,
438 1999).

439 MIP was used to study soil compaction, which was found to mainly affect macroporosity
440 (Destain et al., 2016). Since the size of pore necks rather than the size of pores controls the
441 movement of organisms in soil, MIP appears also suitable for studying the habitat for
442 biological activity function (Elliott and Coleman, 1988). Given that mercury is a non-wetting
443 fluid, the mercury intrusion process is equivalent to air intrusion during water desorption.
444 Therefore, at low pressures, the volume of pores not intruded by mercury could be used to
445 deduce the volume of water held at a given matric potential, i.e., the water retention curve
446 (Romero and Simms, 2008). However, discrepancies were observed (Otalvaro et al., 2016;
447 Ragab et al., 1982). They may be due to the distinct soil volumes investigated, typically
448 bigger for the water retention curve determination, leading to different accessibility of pores,
449 and to a modification of soil structure (swelling-shrinking) during the water retention curve
450 determination or the drying of soil samples (Romero and Simms, 2008).

451 3.1.2. Water retention curve and derived indicators

452 The pore size distribution can also be derived from the water retention curve, i.e., the relation
453 between soil water content (θ) and matric potential (ψ), using water as the probe molecule
454 (Dexter, 1988; Nimmo, 2005). To do so, the measured water retention curve $\theta = f(\psi)$ needs to
455 be first converted into an equivalent $\theta = f(d)$ curve, with d the maximum water-filled pore
456 diameter, according to the Young-Laplace law and assuming a parallel bundle of cylindrical
457 pores. The derivative of this curve provides an estimation of an “equivalent” pore size
458 distribution (Nimmo, 2005), with the same restriction as for MIP.

459 Several methods are available to measure the water retention curve, depending on the sample
460 size and the range of matric potential investigated (Dane and Hopmans 2002). They mainly
461 differ in the way water is extracted, i.e., hanging water column, suction table, pressure plate
462 extractor, or evaporation method. These traditional methods are however prone to error in the
463 dry range, and can thus be complemented by methods based on relative humidity or osmotic

464 equilibration. At tensions close to zero there may be artifacts related to the height of the soil
465 sample. The time required for measuring a water retention curve is usually much longer than
466 for MIP, because of the longer equilibration times. Sample sizes range from a few centimeter
467 clods to cylinders of a few decimeters in diameter. As with MIP, water retention curves are
468 typically hysteretic with separated wetting and drying paths (Dane and Hopmans, 2002). In
469 most applications, the drying path is considered after slow capillary rise to full saturation.
470 Before converting experimental points into a pore size distribution, a model is adjusted (see
471 Kosugi et al., 2002 for a description of these models). This additional step allows an
472 interpolation between experimental points, but can also introduce errors in the estimation of
473 the pore size distribution in case of a poor fitting quality. It is also worth noting that a
474 considerable number of pedotransfer functions exists, to estimate the water retention curve
475 from basic soil properties, e.g., texture, BD, and SOM content, as reviewed by Vereecken et
476 al. (2010).

477 The macropore, mesopore, or micropore volumes can be estimated from defined points on the
478 water retention curve (e.g., Kuncoro et al., 2014; Regelink et al., 2015; Reynolds et al., 2009).
479 These points depend on the chosen size limits for the pore size classes, for which there are no
480 generally agreed upon limits. They are calculated from the matric potential and the Young-
481 Laplace equation. To characterize the pore size distribution, location descriptors such as the
482 mode, median and mean, and shape descriptors such as skewness (asymmetry) and kurtosis
483 (peakedness) were used (Pulido Moncada et al., 2014a; Reynolds et al., 2009). According to
484 Pulido Moncada et al. (2014a), location descriptors providing information on the modal,
485 median, or mean pore size are more informative. Reynolds et al. (2009) proposed an optimal
486 pore structure characterized by a large standard deviation of equivalent pore diameters, a
487 substantial skew towards small pore diameters, and modal pore diameters between 60 and
488 140 μm .

489 The water retention curve can be used to derive a variety of additional indicators (Figure 4),
490 without any transformation into pore size distribution. Saturated water content equals total
491 porosity when the soil is fully saturated (without entrapped air). Air capacity is defined as the
492 volume of air measured when the soil is at field capacity (e.g., Pulido Moncada et al., 2014c;
493 Reynolds et al., 2009). It is used to characterize aeration for plant roots. The relative field
494 capacity corresponds to the water content at field capacity, divided by the saturated water
495 content, and represents the ability of soils to store water and air (e.g., Pulido Moncada et al.,
496 2013; Reynolds et al., 2009). The hypothesis is that soils with relative field capacity between
497 0.6 and 0.7 are likely to have desirable water and air contents for long time periods, which is
498 favorable for nitrogen cycling by micro-organisms and plants (Reynolds et al., 2009). The
499 available water capacity is the ability of soils to store and provide water available to plant
500 roots, measured as the amount of water held between field capacity and permanent wilting
501 point (e.g., Pulido Moncada et al., 2013; Reynolds et al., 2009). Field capacity is, however, a
502 concept not well defined, and is usually measured at matric potentials of 100 or 330 hPa. This
503 choice was discussed to depend on soil texture (e.g., Zacharias and Bohne, 2008).

504 Macropore volume, air capacity, relative field capacity, and available water capacity were
505 deemed to be suitable to discriminate soils of “good” and “poor” physical quality for crop
506 production (Reynolds et al., 2009): non-optimal soils showed poor aeration capacity
507 (excessive water retention) or insufficient capacity to store water available for plants. Air
508 capacity and available water capacity also demonstrated a good sensitivity to management
509 practices (Moebius et al., 2007; Pulido Moncada et al., 2014c). Considering the macropore
510 volume, it was often observed to be affected by compaction, whereas the micropore volume
511 remained unaffected (Kuncoro et al., 2014). As already mentioned for MIP, the pore neck size
512 is probably more useful to describe the movement of organisms in soil than the pore diameter
513 (Elliott and Coleman, 1988). So, by using water retention curves, pore neck sizes were well

514 correlated to the bacterial biomass and diversity and nematode biomass (Hassink et al., 1993;
515 Ruamps et al., 2011). Such good correlations were not observed for fungi and protozoa,
516 because they are able to prospect a large range of pore diameters.

517 The concept of least limiting water range (LLWR), introduced by da Silva et al. (1994) as an
518 index of soil structural quality, goes beyond the definition of available water capacity. In
519 order to characterize the crop production function, LLWR was defined as the range of water
520 contents within which limitations for plant growth associated with water potential, aeration,
521 and mechanical resistance are minimal (da Silva et al., 1994). To determine the critical limit
522 towards the dry range, water content at permanent wilting point and penetration resistance are
523 taken into account. The critical limit towards the wet range is obtained from water content at
524 field capacity and air capacity (Figure 5). These critical limits are usually obtained from the
525 literature (e.g., Asgarzadeh et al., 2010; Kaufmann et al., 2010). To simplify the determination
526 of LLWR, pedotransfer functions were developed to predict LLWR from BD, clay, SOM
527 contents, and cementing agents (da Silva and Kay, 1997; Neyshabouri et al., 2014). It is
528 possible to find a large number of studies using LLWR to examine the effect of different
529 management practices or land uses. However, De Jong van Lier and Gubiani (2015) stated
530 that LLWR does not include the current knowledge of the physical and biological processes
531 occurring during crop growth, so that LLWR did not prove to be efficient to explain crop
532 yields. These authors argue that the wet and dry critical limits are often chosen to be fixed
533 values, whereas these limits are functions of time, depth, and also soil type and plant
534 physiology.

535 The S index developed by Dexter (2004a) is another indicator derived from the water
536 retention curve, intending to represent soil physical quality. It is calculated as the slope of the
537 water retention curve $W = f(\ln |\psi|)$ at its inflection point (with W , the gravimetric water
538 content). By definition, the peak of the pore size distribution derived from the water retention

539 curve corresponds to the slope at the inflection point (Reynolds et al., 2009). Thus, the S-
540 theory implicitly assumes a unimodal distribution of the pore sizes. For a van Genuchten
541 (1980) parametrization, the S index is directly related to the parameter n (de Jong van Lier,
542 2014). The postulate of Dexter (2004a) is that the presence of structural pores is essential for
543 soil physical quality, and that textural porosity is little affected by soil management contrary
544 to structural porosity. The value of S is indicative of the extent to which the soil porosity is
545 concentrated into a narrow range of pore sizes (Dexter, 2004a). A low S index corresponds to
546 a structureless soil, whereas a high S index corresponds to a structured soil with many pores
547 of different size (Dexter, 2004a). A threshold of $S = 0.035$ was suggested to distinguish
548 “good” and “poor” soil physical qualities (Dexter, 2004a). An exception appears for sands, for
549 which the S index may be poorly adapted, because of a lack of structural pores (Reynolds et
550 al., 2009).

551 The S index was observed to be positively correlated with root development (except for
552 sands) (Dexter, 2004a; Kaufmann et al., 2010), soil friability (Dexter, 2004b), and unsaturated
553 hydraulic conductivity at the inflection point (Dexter, 2004c). Some relationships with other
554 indicators of soil structure were investigated. Correlations were observed with BD (Dexter,
555 2004a), packing density and LLWR (Asgarzadeh et al., 2010; Kaufmann et al., 2010), relative
556 field capacity, available water capacity, air capacity, macroporosity, structural stability index
557 (Reynolds et al., 2009), and degree of compactness (Naderi-Boldaji and Keller, 2016). No
558 correlation was found with a visual soil evaluation method (Pulido Moncada et al., 2014b).

559 3.1.3. Gas adsorption

560 Like MIP and the water retention curve, physical gas adsorption methods are indirect
561 methods, using probe molecules to derive properties of the soil pore space in the form of
562 adsorption isotherms (Zachara et al., 2016). Since physical adsorption is involved, all surface
563 sites accessible to the probe molecules are theoretically investigated, as opposed to chemical

564 adsorption (Heister, 2014). In soil science applications, adsorptives are mainly dinitrogen (N₂)
565 (e.g., Hall et al., 2013; Zong et al., 2015), CO₂ (e.g., Echeverría et al., 1999; Ravikovitch et
566 al., 2005), and water vapor (e.g., Jozefaciuk et al., 2015). When using N₂, the analysis is
567 performed at 77 K (−196°C). For CO₂, experiments are performed at 273 K (0°C) and for
568 water at 293 K (20°C). The analysis is carried out on small soil samples, about 1 to 5 mm in
569 diameter, and the pore size investigated usually ranges between 1 and 200 nm. Thus, gas
570 adsorption addresses the lower spatial limit for the characterization of soil structure. The
571 required instruments are easily available. However, due to the limitation to very small pore
572 sizes this method is only relevant for some specific studies. In addition, considering this fine
573 spatial resolution, users usually adopt the pore size terminology given by the IUPAC (Sing et
574 al., 2008), rather than the classical terminology used in soil science: macropores are defined
575 as pores with diameters > 50 nm, mesopore diameters are in the range of 2–50 nm, and
576 micropore diameters are < 2 nm. We will follow this classification in the current section. The
577 reproducibility of the method is recognized to be good (Jozefaciuk et al., 2015; Mayer et al.,
578 2004). For example, by using water desorption isotherms, Jozefaciuk et al. (2015) observed
579 differences < 1.7% between isotherms measured in triplicate. Eusterhues (2005) found
580 standard deviations in the range of 2–10% when comparing several N₂ adsorption
581 measurements of the same sample.

582 Prior to the analysis, samples are degassed (under vacuum or with a flowing gas, and heated)
583 to remove adsorbed molecules including water vapor (Sing et al., 2008), e.g., 1 h at 200°C in
584 Séquaris et al. (2010), 150°C overnight in Mayer et al. (2004), 24 h at 120°C in Ravikovitch
585 et al. (2005). Then, the relative pressure p/p^0 is increased in the measurement cell (where p is
586 the partial pressure of the adsorptive and p^0 is its equilibrium vapor pressure at the
587 temperature of the measurement). The quantity of adsorbed gas is calculated from the
588 difference of pressure before and after the establishment of equilibrium, or by weighing in the

589 case of water adsorption (Sing et al., 2008). The relative pressure is then increased by known
590 increments at constant temperature. During these steps, monolayer, then multilayer adsorption
591 occurs. Micropores are filled first, because of high interactions between the adsorbate and the
592 pore walls. The short distance between two micropore walls leads to an overlap of their
593 adsorption potentials, making these sites more energetic (Lowell et al., 2004). Then, during
594 mesopore and macropore filling, adsorption does not only depend on interaction with pore
595 walls, but also on attractive interaction between adsorbates themselves (Lowell et al., 2004).
596 In this case, the space remaining at the center of the pores after multilayer adsorption on their
597 walls is filled. This mechanism is denoted as capillary condensation, i.e., the gas phase
598 condenses to fill pores at a pressure lower than its saturation pressure, a meniscus is formed at
599 the interface with the vapor phase, and the fluid filling the pore is considered as a liquid
600 (Lowell et al., 2004; Sing et al., 2008). Then, desorption curve is obtained by decreasing the
601 relative pressure.

602 The specific surface area is often calculated from the Brunauer-Emmett-Teller model (BET,
603 Brunauer et al., 1938), for a relative pressure ranging between 0.05 and 0.30 (e.g., Hall et al.,
604 2013; Ravikovitch et al., 2005; Zong et al., 2015). It predicts the number of molecules
605 required to form a monolayer on the sample surface. The total pore volume and the mean pore
606 diameter can then be deduced using data close to saturation (e.g., Séquaris et al., 2010).
607 Among other methods, the Barrett-Joyner-Halenda theory (BJH, Barrett et al., 1951) can be
608 used to determine the mesopore volume and the pore size distribution in the mesopore range
609 (e.g., Zong et al., 2015). Because capillary condensation occurs in the mesopore range,
610 leading to the formation of a meniscus at the interface with the vapor phase, the BJH theory
611 assumes that the Kelvin's equation applies during desorption. It relates the vapor pressure in
612 equilibrium with a curved liquid surface to the pore size. The t-plot method (de Boer et al.,
613 1966) can be used to estimate the micropore volume and surface area from N₂ isotherms. The

614 shape of the hysteresis loop formed by the adsorption and desorption paths allows further
615 interpretation of the pore shapes (Sing et al., 2008). Like all indirect methods, several
616 hypotheses need to be presumed for a valid interpretation, among others, the domain of
617 validity in terms of pore sizes and an idealized pore shape (Zachara et al., 2016).

618 Gas adsorption protocols require heating the soil samples. Heating aims at promoting
619 evaporation, but can cause phase changes in some oxides and hydroxides, a loss of water in
620 the interlayers of clay minerals, and presumably a structural reorganization of SOM, as
621 reported in the review of Heister (2014). To prevent changes in oxides and hydroxides, Kaiser
622 and Guggenberger (2003) degassed their air-dried samples at 20°C during 48 h. Moreover, N₂
623 proved to be inadequate to characterize soils with high amounts of SOM, contrary to CO₂
624 (Echeverría et al., 1999; Ravikovitch et al., 2005). According to de Jong and Mittelmeijer-
625 Hazeleger (1996), the surface area of SOM measured with N₂ gas adsorption might be
626 underestimated by two orders of magnitude. This is linked to the slow diffusion of N₂ at 77 K,
627 which restricts its adsorption in small pores of SOM (de Jonge and Mittelmeijer-Hazeleger,
628 1996; Echeverría et al., 1999; Ravikovitch et al., 2005). In addition, differences were
629 observed between water desorption and N₂ adsorption methods, and explained by the effect of
630 polar water molecules and a modification of the pore structure by the addition of water
631 (Hajnos et al., 2006).

632 A larger specific surface area theoretically provides more reactive sites and thus more
633 possibilities for a substance to interact with the soil solid phase (Heister, 2014). In particular,
634 a correlation was sometimes found between SOM content and specific surface area measured
635 with N₂ adsorption, after SOM destruction (e.g., Kaiser and Guggenberger, 2003; Séquaris et
636 al., 2010). This correlation may be related to the preferential association of SOM with clay
637 particle edges and oxyhydroxides (Kaiser and Guggenberger, 2003; Mayer et al., 2004).
638 However, because SOM adsorption occurs at specific reactive sites, i.e., in patches rather than

639 as a continuous coating (Kaiser and Guggenberger, 2003), this relationship may be too weak
640 to correlate specific surface area to the carbon storage function. For the same reason,
641 micropore and mesopore volumes measured with N₂ adsorption cannot be interpreted as
642 reliable indicators of carbon storage either (Eusterhues et al., 2005; Mayer et al., 2004). The
643 pore sizes resolved with gas adsorption are so small that the majority of the surface area is
644 unavailable for microbial colonization (Darbyshire et al., 1993) and water is only extracted
645 from pores in the investigated size range at pF > 4.2.

646 **3.2. Direct methods**

647 Imaging techniques are considered here as direct methods, since they allow for the evaluation
648 of the soil pore space by direct geometric visualization. Thin sections and serial sections
649 observed by optical microscopes have been used for decades to provide 2-D and 3-D
650 representations of the soil pore network (e.g., Pagliai et al., 2004; Skvortsova and Sanzharova,
651 2007). Next to optical microscopy, scanning electron microscopy (SEM) in backscattered
652 electron mode can be used for structural analyses (e.g., Bruand and Cousin, 1995; Richard et
653 al., 2001). This method requires sample preparation in thin sections. Other methods use
654 radiations interacting with the atoms constituting soil, with the advantage of being non-
655 destructive for soil structure. Examples are X-ray tomography (Cnudde and Boone, 2013;
656 Wildenschild and Sheppard, 2013), gamma-ray tomography (e.g., Pires et al., 2005), neutron
657 tomography (e.g., Schaap et al., 2008; Tumlinson et al., 2008), and nuclear magnetic
658 resonance imaging (e.g., Pohlmeier et al., 2008; Sněhota et al., 2010). The latter two methods
659 are rather efficient to image the water phase.

660 Stereological methods are used to retrieve 3-D information from 2-D images or descriptors
661 are calculated directly from reconstructed 3-D images. In any case, images always need to be
662 processed and optimized for subsequent quantitative analysis. A preprocessing step often

663 consists in applying spatial registration, noise and/or artefact removal, or edge enhancement,
664 as reviewed by Schlüter et al. (2014) and Tuller et al. (2013). Then, if contrast is satisfactory,
665 the segmentation step allows distinguishing different phases as air, water, soil matrix, roots,
666 or gravels. Matrix is here defined as the solid phase including pores (water- and air-filled)
667 with a size lower than the image resolution. The size of the soil sample usually depends on the
668 resolution to be achieved and on the imaging technique used (Wildenschild et al., 2002):
669 resolution can range, for example, from about hundred micrometers using a medical X-ray
670 scanner on a decimeter sample, to a few micrometers using synchrotron-based X-ray
671 tomography on a few millimeter sample. Generally, the ratio between voxel size and sample
672 size is constrained by the properties of the detector panel and ranges between 500 and 2000.

673 First, images can be described visually in a qualitative way, by classifying voids with a
674 typology based on their origin, e.g., biogenic pores, cracks, or textural voids (Skvortsova and
675 Utkaeva, 2008). But the strength of imaging techniques rather lies in the plethora of
676 quantitative morphological and topological descriptors which can be extracted from the
677 images (Helliwell et al., 2013). In contrast to the indirect methods to characterize the soil pore
678 space (section 3.1), meaningful measures such as porosity, pore size distribution, and
679 interfacial area can be retrieved directly, without any assumptions on the pore shape. Some
680 other basic descriptors are the number, length, shape, and orientation of pores (Horgan, 1998;
681 Skvortsova and Utkaeva, 2008). These descriptors are often highly correlated. Some other
682 descriptors characterize the tortuosity, connectivity, or percolation threshold (Renard and
683 Allard, 2013; Vogel et al., 2010). When considering the percolation of the air-phase, the
684 percolation threshold is defined as the lowest porosity at which two opposite faces of the
685 sample are connected by a continuous path. Below this threshold, transport in the air-phase is
686 limited. More complex indicators can be computed to distinguish geometric shape classes of
687 soil pores, from fissure-like to rounded pores (Skvortsova and Sanzharova, 2007), or the

688 distance from any point of the water-filled soil matrix to the closest air-filled pore (Schlüter
689 and Vogel, 2016). This latter indicator can be used to estimate the diffusion length of oxygen,
690 which provides essential information on the redox conditions for microbial activity. All of
691 these descriptors can be calculated on the total pore network, on pores connected to soil
692 surface, or on isolated pores (e.g., Garbout et al., 2013), and in several directions to observe
693 the presence of potential gradients (e.g., Katuwal et al., 2015). By repeating the calculation of
694 a given descriptor on volumes of increasing sizes, it is also possible to evaluate the
695 representative elementary volume of a given descriptor (e.g., Baveye et al., 2002; Costanza-
696 Robinson et al., 2011; Vogel et al., 2002). This can only be performed through non-
697 destructive imaging techniques.

698 However, imaging techniques require expensive instrumentations, expertise, and computing
699 power for image analyses. The segmentation step is particularly sensitive to subjective errors,
700 and its quality directly affects the calculated metrics (Schlüter et al., 2014; Tuller et al., 2013).
701 Various segmentation methods are available, from fully automated to completely operator-
702 dependent. They can lead to very different segmented images, depending on both the method
703 and operator (Baveye et al., 2010). This lack of standard protocol limits comparisons between
704 studies (Helliwell et al., 2013), but no method appears ideal to be applied to a wide range of
705 porous media (Tuller et al., 2013). The segmentation step is especially hindered by noise and
706 partial volume effects, i.e., a blur at object boundaries, where average values of different
707 objects are observed. Lehmann et al. (2006), using sand and glass beads, demonstrated that
708 partial volume effects only disappear when the image resolution is $< 10\%$ of the mean particle
709 size. Vogel et al. (2010) showed that the uncertainty in quantifying soil structure increases
710 significantly when structural units smaller than about 5 pixels in diameter are interpreted.
711 Once this small-scale information is excluded, image segmentation is far less critical. In the

712 same way, quantifying objects bigger than half of the image size should be avoided, because
713 they are not captured in a representative way (Horgan, 1998).

714 Because the soil pore geometry was observed to be more sensitive to changes in management
715 practices than some bulk measurements like BD (Skvortsova and Utkaeva, 2008), imaging
716 techniques are attractive tools to assess soil functions. A first set of indicators is related to the
717 pore shape and orientation. As an example, the presence of elongated pores and their
718 orientation, was related to water movement and leaching processes (Pagliai and Vignozzi,
719 2002; Skvortsova and Utkaeva, 2008). Pore orientation and elongation were also observed to
720 be sensitive to management practices, such as tillage or amendment application (Pagliai et al.,
721 2004).

722 According to Dal Ferro et al. (2012) and Zong et al. (2015), imaging techniques provide a
723 measure of the pore size distribution which is closer to reality than MIP in the overlapping
724 range of pore sizes, because they are not affected by the ink-bottle effect and do not modify
725 soil structure. However, taking into account the ink-bottle effect may be suitable for the soil
726 function related to water retention and transport. Correlations between macroporosity and air
727 permeability, gas diffusivity, and water transport including preferential flow were found
728 (Katuwal et al., 2015; Larsbo et al., 2014; Naveed et al., 2014b; Paradelo et al., 2016). In the
729 study of Luo et al. (2010), for example, macroporosity explained a greater proportion of
730 variability in saturated hydraulic conductivity than BD. There are also experimental evidences
731 that pores of medium size (in the range $\sim 30\text{--}90\ \mu\text{m}$) might play an important role in carbon
732 loss, because of the conditions of air, water, and nutrient supply they provide for OM
733 decomposition (Ananyeva et al., 2013; Kravchenko et al., 2015; Strong et al., 2004; Toosi et
734 al., 2017). Conversely, small pores may provide a physical protection for OM. As a feedback
735 mechanism, carbon sequestration was observed to increase the volume of mesopores and
736 micropores, therefore reducing the risk of fast transport and leaching in macropores (Larsbo et

737 al., 2016). Porosity and pore size distribution were often observed to be affected by
738 management practices such as tillage, amendment application, crop rotation, or land use
739 (Munkholm et al., 2016; Naveed et al., 2014a; Schlüter et al., 2011).

740 Connectivity of the pore network is also a key parameter for soil biota including plant growth
741 as well as water and gas transport. Connectivity appeared to drive saturated hydraulic
742 conductivity (Luo et al., 2010; Sandin et al., 2017), air permeability (Paradelo et al., 2016),
743 and the release of greenhouse gases (Rabot et al., 2015). In addition, several studies showed
744 that particulate organic matter decomposition was affected by pore characteristics. Indeed, the
745 accessibility for organisms and aeration status were controlled by the pore connectivity to the
746 atmosphere and the pore size (Kravchenko et al., 2015; Negassa et al., 2015; Rabbi et al.,
747 2016). The pore connectivity parameter was observed to be sensitive to tillage, fertilization,
748 and land use (Dal Ferro et al., 2014; Jarvis et al., 2017; Naveed et al., 2014a; Schlüter et al.,
749 2011). However, connectivity estimated through the Euler number was not always considered
750 a good measure of macropore connectivity (Katuwal et al., 2015). Indeed, this metric is highly
751 affected by isolated voxels, like unconnected structural pores and thresholding artifacts
752 (Renard and Allard, 2013). Connectivity can also be quantified with the genus density, which
753 only considers the number of loops or redundant connections used to compute the Euler
754 number (e.g., Paradelo et al., 2016) or the path number, i.e., the number of independent and
755 continuous paths between two boundaries (e.g., Luo et al., 2010). Additional measures of
756 connectivity are based on the percolating network, with high significance for preferential flow
757 and transport processes (Jarvis et al., 2017; Sandin et al., 2017). Jarvis et al. (2017) calculated
758 the percolating pore space (i.e., the volume of pores connected to both the top and bottom of
759 the sample) and the proportion of the pore volume represented by the largest cluster. A cluster
760 is here defined as a group of connected pore voxels. The connection probability or Γ
761 connectivity is the second moment of the cluster size distribution (Jarvis et al., 2017; Renard

762 and Allard, 2013; Schlüter and Vogel, 2016), and equals the square of the percolating pore
763 fraction. It represents the probability that two randomly chosen pore voxels belong to the
764 same cluster (Jarvis et al., 2017). So, F connectivity indicates the probability for a connected
765 pathway to exist, whereas the Euler number indicates how many connected pathways exist or
766 are missing (Herring et al., 2015).

767 It is noteworthy that some imaging techniques were recently developed to be used directly in
768 the field, e.g., the method used by Eck et al. (2016) based on laser triangulation, to extract
769 macropores on a dry soil profile. After correcting the pore widths from a swelling effect, Eck
770 et al. (2016) found a significant correlation with the saturated hydraulic conductivity. This
771 example highlights that scanning at the soil horizon or soil profile scale is relevant to
772 characterize water transfers. There would be a priori no major difference linked to the
773 resolution as compared to a coarse-resolution X-ray scanner and the measurement area is
774 similar to that of a visual profile description. However, a major drawback of this technique is
775 that it only provides a 2-D characterization and not a 3-D characterization like tomographic
776 imaging methods do.

777 **4. Discussion**

778 **4.1. Solid phase vs. pore space perspective**

779 Characterizing soil structure from the perspective of aggregates has been criticized (Baveye,
780 2006; Letey, 1991; Pagliai and Vignozzi, 2002; Young et al., 2001). Although appealing, the
781 aggregate perspective does not seem to be the most appropriate to link soil structure with soil
782 functions and processes. The main reason is that analyzing aggregates is more related to the
783 mechanical stability of soil structure rather than to the structure itself. Of course, stability is
784 an important feature but soil processes acting within a given soil are sensitive to the
785 morphological structure of pores and solid which cannot be addressed based on aggregates.

786 Another reason is methodological. As stated above, aggregate size and stability measurements
787 highly depend on the energy applied. Therefore, results may rather depend on the
788 measurement method used, than on soil structure (Young et al., 2001). Moreover, and more
789 general, Young et al. (2001) questioned the existence of distinct soil aggregates in an
790 undisturbed soil profile. They asserted that aggregates are just the result of how we choose to
791 observe them, by applying a given energy.

792 From that, Baveye (2006), Letey (1991), Pagliai and Vignozzi (2002), and Young et al.
793 (2001) suggested characterizing the pore space, rather than a bed of aggregates. Processes
794 occurring in soil are controlled by the pore shape, pore size distribution, pore surface density,
795 connectivity, tortuosity, and heterogeneity of the pore space in three-dimensions (Pagliai and
796 Vignozzi, 2002; Young et al., 2001). They directly influence storage and movement of water,
797 solutes and gases, and root development (Pagliai and Vignozzi, 2002). Moreover, the pore
798 space perspective offers a continuous analysis of the processes occurring in soils,
799 conveniently managed by models, contrary to the discrete analysis proposed by the aggregate
800 perspective. Morphological characteristics based on undisturbed samples could be the key to
801 incorporate quantitative information on soil structure into models (Kravchenko and Guber,
802 2017).

803 In Figure 6, we compare the result of the manual generation of aggregates of four soil samples
804 varying in texture and land use, as could be done during a field description of soil structure, with
805 cross-section images of undisturbed soil samples obtained with X-ray computed tomography
806 (resolution: 20 μm). We carefully broke apart dry clods by hand, then put the resulting
807 fragments on a piece of paper illuminated from the bottom with a LED light panel. Most of
808 the aggregates produced were subangular and their size depended on the energy applied. On
809 the contrary, huge differences are evident between the four soil samples in the X-ray images,
810 in terms of pore shape formed by microcracks, packing voids, root channels, earthworm

811 burrows with visible porosity ($>20\mu\text{m}$) in the range of 10-16% and vastly different pore size
812 distribution (data not shown). Moreover the soils differ regarding the heterogeneity in soil
813 matrix, i.e. aggregates at all scales in the Kühnfeld soil (a), sand in a fine-textured matrix in
814 the Hadera soil (b) and fine-textured loess in the Bad Lauchstädt (c) and Garzweiler soil (d).
815 These examples highlights the fact that soil structure can be addressed much more precisely
816 by using undisturbed soil samples. Moreover, it has to be noted that these two approaches
817 investigate distinct scales, thus leading to different visible features.

818 **4.2. Comparison between indicators**

819 Methods commonly used for soil structure characterization mainly aim at estimating the soil
820 compactness, aggregate shape, grade, size and stability, or pore network morphology and
821 topology. Their known advantages and limitations are reported in Table 1. Field evaluations
822 of soil structure, based on the fundamental principles of soil surveys, provide valuable
823 information about soil structure. Some of them are fast and cheap, but have the disadvantage
824 of being semi-quantitative and of requiring a trained eye. Measuring the aggregate size
825 distribution and stability is labor-intensive, and suffers from a lack of standard in the sample
826 pretreatment and in the measurement itself. Despite these drawbacks, the use of aggregate size
827 distribution and stability tests is highly valuable in e.g., erosion studies. BD is not considered
828 to be a good indicator for soil functions in general, because it does not take into account
829 important soil structural attributes. Indirect methods to characterize the pore space, such as the
830 water retention curve, MIP, and gas adsorption, all require assumptions on an idealized pore
831 shape to interpret the results. Using an assumption on the pore shape to characterize the pore
832 space is, of course, a questionable approach. Moreover, the water retention curve and MIP are
833 both subject to the ink-bottle effect, a well-known phenomenon not always taken into
834 consideration when interpreting the results. However, because of the implicit consideration of
835 the ink-bottle effect, they might be suitable for studying soil functions related to water

836 retention and transport. In fact, the concept of Mualem (1976) to derive the relative hydraulic
837 conductivity based on the water retention curve is pretty successful, probably because it
838 implicitly includes the ink-bottle effect (Vogel, 2000). Finally, laboratory-based imaging
839 techniques appear to be efficient in characterizing soil structure because they not only allow
840 quantifying the pore volume, pore size distribution, and interfacial area, but also the pore
841 connectivity and pore contact distances, with an additional significance for soil functions.
842 Since these indicators are spatially resolved, the presence of gradients can be studied and
843 calculations can be restricted to a given group of pores relevant for the soil function under
844 consideration (e.g., connected to soil surface). Imaging techniques used in the field are
845 promising since they allow scanning large areas, but they only provide a 2-D characterization
846 of a soil profile.

847 Throughout this review, we gathered evidences that soil moisture conditions could be an
848 obstacle to evaluate and compare a given indicator at any period of the year. Indeed, a
849 significant modification of soil structure is often observed after wetting and after drying a soil
850 sample, because of swelling and shrinking phenomena (Della Vecchia et al., 2015; Simms and
851 Yanful, 2001). This highlights the dependency of the pore size distribution to the soil water
852 content. To address this problem, aggregate size distribution and aggregate stability tests often
853 use dry or rewetted soil samples to establish standard conditions of soil moisture and hydric
854 history, but with possible damaging effects on soil structure (Dexter, 1988). Eck et al. (2016)
855 normalized the pore diameters measured under dry conditions by the coefficient of linear
856 extensibility, to retrieve the macropore diameters that would be measured at saturation. MIP
857 and gas adsorption methods also use dry samples. With respect to pore space morphology,
858 however, none of these methods appears actually able to provide reliable information using a
859 single measurement.

860 Some of these methods are themselves sensitive to soil texture or SOM content because they
861 require the breakdown of aggregates. Additionally, a specific bulk density would not be
862 interpreted the same way in a sandy and a clayey soil, because the aggregation of primary
863 particles is extremely different. On the contrary, the metrics derived from imaging are
864 measured independently of the aggregation process and can thus be interpreted directly. For
865 these reasons, to use soil structure as an efficient indicator of soil functions, it is necessary to
866 characterize the pore space of undisturbed soil samples.

867 The indicators presented in this review are evaluated according to their relevance to the
868 investigated soil functions in Table 2. Unsurprisingly, several indicators of soil structure are
869 able to characterize the function related to the storage and filtering of water. The habitat for
870 biological activity function appeared to be quite conveniently assessed by using indirect
871 methods subject to the ink-bottle effect. On the contrary, the storage and recycling of nutrients
872 and carbon storage functions are more difficult to assess with indicators of soil structure since
873 these functions also involve chemical reactions. However, some indicators controlling water
874 movement and erosion, such as the macroporosity, pore orientation, pore connectivity, and
875 stability index allow for characterizing these two soil functions at least partly. The major
876 difficulty in assessing the biomass production function (i.e., soil fertility) is that critical
877 thresholds of indicators are expected to depend on plant physiology. Finally, the physical
878 stability and support function is mostly assessed through aggregate stability tests. Considering
879 the methodological limitations discussed above, porosity, macroporosity, and pore
880 connectivity appear to be the most relevant indicators for several soil functions.

881 **4.3. A need for a soil structure library**

882 One major conclusion of this review is that pore network characterization based on
883 undisturbed samples is much more powerful to assess soil functions as compared to the

884 analysis of disturbed aggregates. Today, excellent tools exist to quantify soil structure using
885 non-destructive tomographic techniques (mainly X-ray computed tomography). However,
886 these tools are restricted to specialized labs and are not widely applicable to characterize field
887 soils. On the other hand, a wide number of field methods and simple lab tools are accessible
888 but their applications are highly subjective and many protocols depend on boundary
889 conditions which are hard to control (e.g., actual soil water content). This poses a fundamental
890 dilemma.

891 Since imaging techniques are not accessible outside of a research context, effort should be
892 made to produce knowledge about structural characteristics for a large range of soil types in
893 connection to their functional characteristics. This will allow for an extended exploration of
894 how soil structure is related to soil functions. As a first step, we suggest developing
895 standardized protocols to quantify soil structure based on undisturbed imaging in terms of
896 pore morphology and topology. In a next step, an open access “soil structure library” could be
897 established, gathering information on the selected indicators together with their metadata (i.e.,
898 imaging technique, sampled volume, image resolution), a site and soil characterization (e.g.,
899 soil type, texture, SOM content, sampling depth, etc.), and complementary soil properties
900 (e.g., other indicators of soil structure, saturated hydraulic conductivity, air permeability, etc.).
901 Finally, through this database, it will become possible to establish relationships between
902 selected indicators of undisturbed soil structure with simpler indicators of soil structure in a
903 site-specific way. This has, to some extent, the potential to solve the above mentioned
904 dilemma and will be the subject of a forthcoming paper.

905 **5. Conclusion**

906 In this review, we intended to identify relevant indicators of soil structure to assess soil
907 functions. We identified porosity, macroporosity, and pore connectivity as relevant for several

908 soil functions. Imaging instruments appeared to be the most reliable tools to measure them.
909 Up to now, imaging techniques demonstrated their efficiencies, essentially to characterize
910 water dynamics, and so the soil function related to water storage and transport of non-reactive
911 substances. New insights also emerged recently for the carbon storage function, recognizing a
912 more important role to the physical protection of SOM. Additional knowledge could be
913 gathered by broadening the questions tackled using imaging techniques, for example about the
914 physical stability and support function. In this review, we did not draw any conclusions about
915 the exact type of relationships between the selected indicators and soil functions, but we
916 reduced considerably the number of soil structural properties to be included in a meta-
917 analysis. We believe that these relationships are typically not linear, thus requiring reviewing
918 a very large amount of studies on different soil types and management practices to span the whole
919 range of these properties and to draw reliable conclusions. Since imaging techniques are not
920 accessible outside of a research context, effort should be made to produce knowledge for a
921 large range of soil types through a “soil structure library”, in order to characterize and derive
922 relationships for soils of similar functioning.

923 **Acknowledgments**

924 This work was funded by the German Federal Ministry of Education and Research (BMBF) in
925 the framework of the funding measure “Soil as a Sustainable Resource for the Bioeconomy –
926 BonaRes”, project “BonaRes (Module B): BonaRes Centre for Soil Research, subprojects A
927 and C” (grants 031A608A and 031A608C).

928 **References**

929 Ad-hoc-AG Boden, 2005. Bodenkundliche Kartieranleitung (KA 5). Schweizerbart, Stuttgart.
930 Almajmaie, A., Hardie, M., Acuna, T., Birch, C., 2017. Evaluation of methods for

- 931 determining soil aggregate stability. *Soil Tillage Res.* 167, 39–45.
932 doi:10.1016/j.still.2016.11.003
- 933 Ananyeva, K., Wang, W., Smucker, A.J.M., Rivers, M.L., Kravchenko, A.N., 2013. Can
934 intra-aggregate pore structures affect the aggregate's effectiveness in protecting carbon?
935 *Soil Biol. Biochem.* 57, 868–875. doi:10.1016/j.soilbio.2012.10.019
- 936 Angers, D.A., Recous, S., Aita, C., 1997. Fate of carbon and nitrogen in water-stable
937 aggregates during decomposition of $^{13}\text{C}^{15}\text{N}$ -labelled wheat straw in situ. *Eur. J. Soil Sci.*
938 48, 295–300. doi:10.1111/j.1365-2389.1997.tb00549.x
- 939 Asgarzadeh, H., Mosaddeghi, M.R., Mahboubi, A.A., Nosrati, A., Dexter, A.R., 2010. Soil
940 water availability for plants as quantified by conventional available water, least limiting
941 water range and integral water capacity. *Plant Soil* 335, 229–244. doi:10.1007/s11104-
942 010-0410-6
- 943 Baize, D., Duval, O., Richard, G., 2013. *Les sols et leurs structures. Observations à*
944 *différentes échelles.* Editions Quae, Versailles.
- 945 Baize, D., Jabiol, B., 2011. *Guide pour la description des sols, Collection Savoir-Faire.*
946 Editions Quae.
- 947 Ball, B.C., Batey, T., Munkholm, L.J., 2007. Field assessment of soil structural quality - a
948 development of the Peerlkamp test. *Soil Use Manag.* 23, 329–337. doi:10.1111/j.1473-
949 2743.2007.00102.x
- 950 Ball, B.C., Batey, T., Munkholm, L.J., Guimarães, R.M.L., Boizard, H., McKenzie, D.C.,
951 Peigné, J., Tormena, C.A., Hargreaves, P., 2015. The numeric visual evaluation of
952 subsoil structure (SubVESS) under agricultural production. *Soil Tillage Res.* 148, 85–96.
953 doi:10.1016/j.still.2014.12.005
- 954 Barrett, E.P., Joyner, L.G., Halenda, P.P., 1951. The determination of pore volume and area

955 distributions in porous substances. I. Computations from nitrogen isotherms. *J. Am.*
956 *Chem. Soc.* 73, 373–380. doi:10.1021/ja01145a126

957 Barthès, B., Roose, E., 2002. Aggregate stability as an indicator of soil susceptibility to runoff
958 and erosion; validation at several levels. *Catena* 47, 133–149. doi:10.1016/S0341-
959 8162(01)00180-1

960 Bauer, T., Strauss, P., Murer, E., 2014. A photogrammetric method for calculating soil bulk
961 density. *J. Plant Nutr. Soil Sci.* 177, 496–499. doi:10.1002/jpln.201400010

962 Baveye, P., 2006. Comment on “Soil structure and management: a review” by C.J. Bronick
963 and R. Lal. *Geoderma* 134, 231–232. doi:10.1016/j.geoderma.2005.10.003

964 Baveye, P., Rogasik, H., Wendroth, O., Onasch, I., Crawford, J.W., 2002. Effect of sampling
965 volume on the measurement of soil physical properties: simulation with x-ray
966 tomography data. *Meas. Sci. Technol.* 13, 775–784. doi:10.1088/0957-0233/13/5/316

967 Baveye, P.C., Laba, M., Otten, W., Bouckaert, L., Dello Sterpaio, P., Goswami, R.R., Grinev,
968 D., Houston, A., Hu, Y., Liu, J., Mooney, S., Pajor, R., Sleutel, S., Tarquis, A., Wang,
969 W., Wei, Q., Sezgin, M., 2010. Observer-dependent variability of the thresholding step
970 in the quantitative analysis of soil images and X-ray microtomography data. *Geoderma*
971 157, 51–63. doi:10.1016/j.geoderma.2010.03.015

972 Beare, M.H., Bruce, R.R., 1993. A comparison of methods for measuring water-stable
973 aggregates: implications for determining environmental effects on soil structure.
974 *Geoderma* 56, 87–104. doi:10.1016/0016-7061(93)90102-Q

975 Boizard, H., Peigné, J., Sasal, M.C., de Fátima Guimarães, M., Piron, D., Tomis, V., Vian, J.-
976 F., Cadoux, S., Ralisch, R., Tavares Filho, J., Heddadj, D., De Battista, J., Duparque, A.,
977 Franchini, J.C., Roger-Estrade, J., 2017. Developments in the “profil cultural” method
978 for an improved assessment of soil structure under no-till. *Soil Tillage Res.* 173, 93–103.

- 979 doi:10.1016/j.still.2016.07.007
- 980 Bottinelli, N., Jouquet, P., Capowiez, Y., Podwojewski, P., Grimaldi, M., Peng, X., 2015.
981 Why is the influence of soil macrofauna on soil structure only considered by soil
982 ecologists? *Soil Tillage Res.* 146, 118–124. doi:10.1016/j.still.2014.01.007
- 983 Bruand, A., Cousin, I., 1995. Variation of textural porosity of a clay-loam soil during
984 compaction. *Eur. J. Soil Sci.* 46, 377–385. doi:10.1111/j.1365-2389.1995.tb01334.x
- 985 Brubaker, S.C., Holzhey, C.S., Brasher, B.R., 1992. Estimating the water-dispersible clay
986 content of soils. *Soil Sci. Soc. Am. J.* 56, 1226–1232.
987 doi:10.2136/sssaj1992.03615995005600040036x
- 988 Brunauer, S., Emmett, P.H., Teller, E., 1938. Adsorption of gases in multimolecular layers. *J.*
989 *Am. Chem. Soc.* 60, 309–319. doi:10.1021/ja01269a023
- 990 Calero, N., Barrón, V., Torrent, J., 2008. Water dispersible clay in calcareous soils of
991 southwestern Spain. *Catena* 74, 22–30. doi:10.1016/j.catena.2007.12.007
- 992 Cameron, K.C., Buchan, G.D., 2006. Porosity and pore size distribution, in: Lal, R. (Ed.),
993 *Encyclopedia of Soil Science*. CRC Press, Boca Raton, FL, pp. 1350–1353.
- 994 Christensen, B.T., 2001. Physical fractionation of soil and structural and functional
995 complexity in organic matter turnover. *Eur. J. Soil Sci.* 52, 345–353. doi:10.1046/j.1365-
996 2389.2001.00417.x
- 997 Cnudde, V., Boone, M.N., 2013. High-resolution X-ray computed tomography in
998 geosciences: A review of the current technology and applications. *Earth-Science Rev.*
999 123, 1–17. doi:10.1016/j.earscirev.2013.04.003
- 1000 Costanza-Robinson, M.S., Estabrook, B.D., Fouhey, D.F., 2011. Representative elementary
1001 volume estimation for porosity, moisture saturation, and air-water interfacial areas in

1002 unsaturated porous media: data quality implications. *Water Resour. Res.* 47, 1–12.
1003 doi:10.1029/2010WR009655

1004 Cuisinier, O., Laloui, L., 2004. Fabric evolution during hydromechanical loading of a
1005 compacted silt. *Int. J. Numer. Anal. Methods Geomech.* 28, 483–499.
1006 doi:10.1002/nag.348

1007 Czyż, E.A., Dexter, A.R., 2015. Mechanical dispersion of clay from soil into water: readily-
1008 dispersed and spontaneously-dispersed clay. *Int. Agrophysics* 29, 1–7.
1009 doi:10.1515/intag-2015-0007

1010 da Silva, A.P., Kay, B.D., 1997. Estimating the Least Limiting Water Range of soils from
1011 properties and management. *Soil Sci. Soc. Am. J.* 61, 877–883.
1012 doi:10.2136/sssaj1997.03615995006100030023x

1013 da Silva, A.P., Kay, B.D., Perfect, E., 1997. Management versus inherent soil properties
1014 effects on bulk density and relative compaction. *Soil Tillage Res.* 44, 81–93.
1015 doi:10.1016/S0167-1987(97)00044-5

1016 da Silva, A.P., Kay, B.D., Perfect, E., 1994. Characterization of the Least Limiting Water
1017 Range of soils. *Soil Sci. Soc. Am. J.* 58, 1775–1781.
1018 doi:10.2136/sssaj1994.03615995005800060028x

1019 Dal Ferro, N., Delmas, P., Duwig, C., Simonetti, G., Morari, F., 2012. Coupling X-ray
1020 microtomography and mercury intrusion porosimetry to quantify aggregate structures of
1021 a cambisol under different fertilisation treatments. *Soil Tillage Res.* 119, 13–21.
1022 doi:10.1016/j.still.2011.12.001

1023 Dal Ferro, N., Sartori, L., Simonetti, G., Berti, A., Morari, F., 2014. Soil macro- and
1024 microstructure as affected by different tillage systems and their effects on maize root
1025 growth. *Soil Tillage Res.* 140, 55–65. doi:10.1016/j.still.2014.02.003

- 1026 Dane, J.H., Hopmans, J.W., 2002. Water retention and storage, in: Dane, J.H., Topp, G.C.
1027 (Eds.), *Methods of Soil Analysis. Part 4. Physical Methods*. Soil Science Society of
1028 America, Book Series No. 5, Madison, WI., pp. 671–719.
- 1029 Darbyshire, J.F., Chapman, S.J., Cheshire, M. V., Gauld, J.H., McHardy, W.J., Paterson, E.,
1030 Vaughan, D., 1993. Methods for the study of interrelationships between micro-organisms
1031 and soil structure. *Geoderma* 56, 3–23. doi:10.1016/0016-7061(93)90097-5
- 1032 de Boer, J.H., Lippens, B.C., Linsen, B.G., Broekhoff, J.C.P., van den Heuvel, A., Osinga,
1033 T.J., 1966. The t-curve of multimolecular N₂-adsorption. *J. Colloid Interface Sci.* 21,
1034 405–414. doi:10.1016/0095-8522(66)90006-7
- 1035 de Jong van Lier, Q., 2014. Revisiting the S-index for soil physical quality and its use in
1036 Brazil. *Rev. Bras. Cienc. Do Solo* 38, 1–10. doi:10.1590/S0100-06832014000100001
- 1037 de Jong van Lier, Q., Gubiani, P.I., 2015. Beyond the “Least Limiting Water Range”:
1038 rethinking soil physics research in Brazil. *Rev. Bras. Cienc. do Solo* 39, 925–939.
1039 doi:10.1590/01000683rbc20140596
- 1040 de Jonge, H., Mittelmeijer-Hazeleger, M.C., 1996. Adsorption of CO₂ and N₂ on soil organic
1041 matter: nature of porosity, surface area, and diffusion mechanisms. *Environ. Sci.*
1042 *Technol.* 30, 408–413. doi:10.1021/es950043t
- 1043 de Oliveira, P.D., Sato, M.K., de Lima, H.V., Rodrigues, S., da Silva, A.P., 2016. Critical
1044 limits of the degree of compactness and soil penetration resistance for the soybean crop
1045 in N Brazil. *J. Plant Nutr. Soil Sci.* 179, 78–87. doi:10.1002/jpln.201400315
- 1046 Delage, P., Pellerin, F.M., 1984. Influence de la lyophilisation sur la structure d’une argile
1047 sensible du Québec. *Clay Miner.* 19, 151–160. doi:10.1180/claymin.1984.019.2.03
- 1048 Della Vecchia, G., Dieudonné, A.C., Jommi, C., Charlier, R., 2015. Accounting for evolving
1049 pore size distribution in water retention models for compacted clays. *Int. J. Numer. Anal.*

1050 Methods Geomech. 39, 702–723. doi:10.1002/nag.2326

1051 Denef, K., Six, J., Merckx, R., Paustian, K., 2004. Carbon sequestration in microaggregates of
1052 no-tillage soils with different clay mineralogy. Soil Sci. Soc. Am. J. 68, 1935–1944.
1053 doi:10.2136/sssaj2004.1935

1054 Denef, K., Zotarelli, L., Boddey, R.M., Six, J., 2007. Microaggregate-associated carbon as a
1055 diagnostic fraction for management-induced changes in soil organic carbon in two
1056 Oxisols. Soil Biol. Biochem. 39, 1165–1172. doi:10.1016/j.soilbio.2006.12.024

1057 Destain, M.F., Roisin, C., Dalcq, A.S., Mercatoris, B.C.N., 2016. Effect of wheel traffic on
1058 the physical properties of a Luvisol. Geoderma 262, 276–284.
1059 doi:10.1016/j.geoderma.2015.08.028

1060 Dexter, A.R., 2004a. Soil physical quality Part I. Theory, effects of soil texture, density, and
1061 organic matter, and effects on root growth. Geoderma 120, 201–214.
1062 doi:10.1016/j.geoderma.2003.09.004

1063 Dexter, A.R., 2004b. Soil physical quality: Part II. Friability, tillage, tith and hard-setting.
1064 Geoderma 120, 215–225. doi:10.1016/j.geoderma.2003.09.005

1065 Dexter, A.R., 2004c. Soil physical quality. Part III: Unsaturated hydraulic conductivity and
1066 general conclusions about S-theory. Geoderma 120, 227–239.
1067 doi:10.1016/j.geoderma.2003.09.006

1068 Dexter, A.R., 1988. Advances in characterization of soil structure. Soil Tillage Res. 11, 199–
1069 238. doi:10.1016/0167-1987(88)90002-5

1070 Diamond, S., 1970. Pore size distributions in clays. Clays Clay Miner. 18, 7–23.
1071 doi:10.1346/CCMN.1970.0180103

1072 Díaz-Zorita, M., Perfect, E., Grove, J.H., 2002. Disruptive methods for assessing soil

1073 structure. *Soil Tillage Res.* 64, 3–22. doi:10.1016/S0167-1987(01)00254-9

1074 Drury, C.F., Yang, X.M., Reynolds, W.D., Tan, C.S., 2004. Influence of crop rotation and
1075 aggregate size on carbon dioxide production and denitrification. *Soil Tillage Res.* 79,
1076 87–100. doi:10.1016/j.still.2004.03.020

1077 Echeverría, J.C., Morera, M.T., Mazkaran, C., Garrido, J.J., 1999. Characterization of the
1078 porous structure of soils: adsorption of nitrogen (77K) and carbon dioxide (273K), and
1079 mercury porosimetry. *Eur. J. Soil Sci.* 50, 497–503. doi:10.1046/j.1365-
1080 2389.1999.00261.x

1081 Eck, D. V., Qin, M., Hirmas, D.R., Giménez, D., Brunsell, N.A., 2016. Relating quantitative
1082 soil structure metrics to saturated hydraulic conductivity. *Vadose Zone J.* 15.
1083 doi:10.2136/vzj2015.05.0083

1084 Elliott, E.T., Coleman, D.C., 1988. Let the soil work for us. *Ecol. Bull.* 39, 23–32.

1085 Eusterhues, K., Rumpel, C., Kögel-Knabner, I., 2005. Organo-mineral associations in sandy
1086 acid forest soils: importance of specific surface area, iron oxides and micropores. *Eur. J.*
1087 *Soil Sci.* 56, 753–763. doi:10.1111/j.1365-2389.2005.00710.x

1088 FAO, 2006. Guidelines for soil description, 4th ed. Food and Agriculture Organisation of the
1089 United Nations, Rome, Italy.

1090 Feeney, D.S., Crawford, J.W., Daniell, T., Hallett, P.D., Nunan, N., Ritz, K., Rivers, M.,
1091 Young, I.M., 2006. Three-dimensional microorganization of the soil-root-microbe
1092 system. *Microb. Ecol.* 52, 151–158. doi:10.1007/s00248-006-9062-8

1093 Fiès, J.C., 1984. Analyse de la répartition du volume des pores dans les assemblages argile-
1094 squelettes : comparaison entre un modèle d'espace poral textural et les données fournies
1095 par la porosimétrie au mercure. *Agronomie* 9, 891–899.

- 1096 Frisbie, J.A., Graham, R.C., Lee, B.D., 2014. A plaster cast method for determining soil bulk
1097 density. *Soil Sci.* 179, 103–106. doi:10.1097/SS.0000000000000044
- 1098 Garbout, A., Munkholm, L.J., Hansen, S.B., 2013. Tillage effects on topsoil structural quality
1099 assessed using X-ray CT, soil cores and visual soil evaluation. *Soil Tillage Res.* 128,
1100 104–109. doi:10.1016/j.still.2012.11.003
- 1101 Giarola, N.F.B., da Silva, Á.P., Tormena, C.A., Guimarães, R.M.L., Ball, B.C., 2013. On the
1102 Visual Evaluation of Soil Structure: the Brazilian experience in Oxisols under no-tillage.
1103 *Soil Tillage Res.* 127, 60–64. doi:10.1016/j.still.2012.03.004
- 1104 Giesche, H., 2006. Mercury porosimetry: a general (practical) overview. Part. Part. Syst.
1105 Charact. 23, 9–19. doi:10.1002/ppsc.200601009
- 1106 Guimarães, R.M.L., Ball, B.C., Tormena, C.A., 2011. Improvements in the visual evaluation
1107 of soil structure. *Soil Use Manag.* 27, 395–403. doi:10.1111/j.1475-2743.2011.00354.x
- 1108 Guimarães, R.M.L., Ball, B.C., Tormena, C.A., Giarola, N.F.B., da Silva, Á.P., 2013.
1109 Relating visual evaluation of soil structure to other physical properties in soils of
1110 contrasting texture and management. *Soil Tillage Res.* 127, 92–99.
1111 doi:10.1016/j.still.2012.01.020
- 1112 Guimarães, R.M.L., Lamandé, M., Munkholm, L.J., Ball, B.C., Keller, T., 2017.
1113 Opportunities and future directions for visual soil evaluation methods in soil structure
1114 research. *Soil Tillage Res.* 173, 104–113. doi:10.1016/j.still.2017.01.016
- 1115 Hajnos, M., Lipiec, J., Świeboda, R., Sokołowska, Z., Witkowska-Walczak, B., 2006.
1116 Complete characterization of pore size distribution of tilled and orchard soil using water
1117 retention curve, mercury porosimetry, nitrogen adsorption, and water desorption
1118 methods. *Geoderma* 135, 307–314. doi:10.1016/j.geoderma.2006.01.010
- 1119 Håkansson, I., 1990. A method for characterizing the state of compactness of the plough

- 1120 layer. *Soil Tillage Res.* 16, 105–120. doi:10.1016/0167-1987(90)90024-8
- 1121 Håkansson, I., Lipiec, J., 2000. A review of the usefulness of relative bulk density values in
1122 studies of soil structure and compaction. *Soil Tillage Res.* 53, 71–85.
1123 doi:10.1016/S0167-1987(99)00095-1
- 1124 Hall, M.R., Mooney, S.J., Sturrock, C., Matelloni, P., Rigby, S.P., 2013. An approach to
1125 characterisation of multi-scale pore geometry and correlation with moisture storage and
1126 transport coefficients in cement-stabilised soils. *Acta Geotech.* 8, 67–79.
1127 doi:10.1007/s11440-012-0178-3
- 1128 Han, L., Sun, K., Jin, J., Xing, B., 2015. Some concepts of soil organic carbon characteristics
1129 and mineral interaction from a review of literature. *Soil Biol. Biochem.* 94, 107–121.
1130 doi:10.1016/j.soilbio.2015.11.023
- 1131 Harrison, R.B., Adams, A.B., Licata, C., Flaming, B., Wagoner, G.L., Carpenter, P., Vance,
1132 E.D., 2003. Quantifying deep-soil and coarse-soil fractions: avoiding sampling bias. *Soil*
1133 *Sci. Soc. Am. J.* 67, 1602–1606.
- 1134 Hassink, J., Bouwman, L.A., Zwart, K.B., Brussaard, L., 1993. Relationships between
1135 habitable soil biota and mineralization rates in grassland soils. *Soil Biol. Biochem.* 25,
1136 47–55. doi:10.1016/0038-0717(93)90240-C
- 1137 Haynes, R.J., 1993. Effect of sample pretreatment on aggregate stability measured by wet
1138 sieving or turbidimetry on soils of different cropping history. *J. Soil Sci.* 44, 261–270.
1139 doi:10.1111/j.1365-2389.1993.tb00450.x
- 1140 Heister, K., 2014. The measurement of the specific surface area of soils by gas and polar
1141 liquid adsorption methods - Limitations and potentials. *Geoderma* 216, 75–87.
1142 doi:10.1016/j.geoderma.2013.10.015
- 1143 Helliwell, J.R., Sturrock, C.J., Grayling, K.M., Tracy, S.R., Flavel, R.J., Young, I.M.,

- 1144 Whalley, W.R., Mooney, S.J., 2013. Applications of X-ray computed tomography for
1145 examining biophysical interactions and structural development in soil systems: a review.
1146 *Eur. J. Soil Sci.* 64, 279–297. doi:10.1111/ejss.12028
- 1147 Herring, A.L., Andersson, L., Schlüter, S., Sheppard, A., Wildenschild, D., 2015. Efficiently
1148 engineering pore-scale processes: The role of force dominance and topology during
1149 nonwetting phase trapping in porous media. *Adv. Water Resour.* 79, 91–102.
1150 doi:10.1016/j.advwatres.2015.02.005
- 1151 Holmes, K.W., Wherrett, A., Keating, A., Murphy, D.V., 2011. Meeting bulk density
1152 sampling requirements efficiently to estimate soil carbon stocks. *Soil Res.* 49, 680–695.
1153 doi:10.1071/SR11161
- 1154 Horgan, G.W., 1998. Mathematical morphology for analysing soil structure from images. *Eur.*
1155 *J. Soil Sci.* 49, 161–173. doi:10.1046/j.1365-2389.1998.00160.x
- 1156 Igwe, C.A., Udegbonam, O.N., 2008. Soil properties influencing water-dispersible clay and
1157 silt in an Ultisol in southern Nigeria. *Int. Agrophysics* 22, 319–325.
- 1158 ISO 10930, 2012. Soil quality — Measurement of the stability of soil aggregates subjected to
1159 the action of water.
- 1160 Jarvis, N., Larsbo, M., Koestel, J., 2017. Connectivity and percolation of structural pore
1161 networks in a cultivated silt loam soil quantified by X-ray tomography. *Geoderma* 287,
1162 71–79. doi:10.1016/j.geoderma.2016.06.026
- 1163 Jozefaciuk, G., Czachor, H., Lamorski, K., Hajnos, M., Swieboda, R., Franus, W., 2015.
1164 Effect of humic acids, sesquioxides and silica on the pore system of silt aggregates
1165 measured by water vapour desorption, mercury intrusion and microtomography. *Eur. J.*
1166 *Soil Sci.* 66, 992–1001. doi:10.1111/ejss.12299
- 1167 Kaiser, K., Guggenberger, G., 2003. Mineral surfaces and soil organic matter. *Eur. J. Soil Sci.*

1168 54, 219–236. doi:10.1046/j.1365-2389.2003.00544.x

1169 Katuwal, S., Norgaard, T., Moldrup, P., Lamandé, M., Wildenschild, D., de Jonge, L.W.,
1170 2015. Linking air and water transport in intact soils to macropore characteristics inferred
1171 from X-ray computed tomography. *Geoderma* 237–238, 9–20.
1172 doi:10.1016/j.geoderma.2014.08.006

1173 Kaufmann, M., Tobias, S., Schulin, R., 2010. Comparison of critical limits for crop plant
1174 growth based on different indicators for the state of soil compaction. *J. Plant Nutr. Soil*
1175 *Sci.* 173, 573–583. doi:10.1002/jpln.200900129

1176 Keller, T., Håkansson, I., 2010. Estimation of reference bulk density from soil particle size
1177 distribution and soil organic matter content. *Geoderma* 154, 398–406.
1178 doi:10.1016/j.geoderma.2009.11.013

1179 Kemper, W.D., Rosenau, R.C., 1984. Soil cohesion as affected by time and water content.
1180 *Soil Sci. Soc. Am. J.* 48, 1001–1006.
1181 doi:doi:10.2136/sssaj1984.03615995004800050009x

1182 Kjaergaard, C., De Jonge, L.W., Moldrup, P., Schjønning, P., 2004. Water-dispersible
1183 colloids: effects of measurement method, clay content, initial soil matric potential, and
1184 wetting rate. *Vadose Zone J.* 3, 403–412. doi:10.2136/vzj2004.0403

1185 Kloubek, J., 1981. Hysteresis in porosimetry. *Powder Technol.* 29, 63–73. doi:10.1016/0032-
1186 5910(81)85005-X

1187 Kong, A.Y.Y., Six, J., Bryant, D.C., Denison, R.F., van Kessel, C., 2005. The relationship
1188 between carbon input, aggregation, and soil organic carbon stabilization in sustainable
1189 cropping systems. *Sci. Soc. Am. J.* 69, 1078–1085. doi:10.2136/sssaj2004.0215

1190 Kosugi, K., Dane, J.H., Hopmans, J.W., 2002. Parametric models, in: Dane, J.H., Topp, G.C.
1191 (Eds.), *Methods of Soil Analysis. Part 4. Physical Methods.* Soil Science Society of

- 1192 America, Book Series No. 5, Madison, WI., pp. 739–757.
- 1193 Kozak, E., Stawinski, J., Wierzchos, J., 1991. Reliability of mercury intrusion porosimetry
1194 results for soils. *Soil Sci.* 152, 405–413. doi:10.1097/00010694-199112000-00002
- 1195 Kravchenko, A.N., Guber, A.K., 2017. Soil pores and their contributions to soil carbon
1196 processes. *Geoderma* 287, 31–39. doi:10.1016/j.geoderma.2016.06.027
- 1197 Kravchenko, A.N., Negassa, W.C., Guber, A.K., Rivers, M.L., 2015. Protection of soil carbon
1198 within macro-aggregates depends on intra-aggregate pore characteristics. *Sci. Rep.* 5,
1199 16261. doi:10.1038/srep16261
- 1200 Krull, E.S., Baldock, J.A., Skjemstad, J.O., 2003. Importance of mechanisms and processes of
1201 the stabilisation of soil organic matter for modelling carbon turnover. *Funct. Plant Biol.*
1202 30, 207–222. doi:10.1071/FP02085
- 1203 Kuncoro, P.H., Koga, K., Satta, N., Muto, Y., 2014. A study on the effect of compaction on
1204 transport properties of soil gas and water. II: Soil pore structure indices. *Soil Tillage Res.*
1205 143, 180–187. doi:10.1016/j.still.2014.01.008
- 1206 Larsbo, M., Koestel, J., Jarvis, N., 2014. Relations between macropore network characteristics
1207 and the degree of preferential solute transport. *Hydrol. Earth Syst. Sci.* 18, 5255–5269.
1208 doi:10.5194/hess-18-5255-2014
- 1209 Larsbo, M., Koestel, J., Kätterer, T., Jarvis, N., 2016. Preferential transport in macropores is
1210 reduced by soil organic carbon. *Vadose Zone J.* 15. doi:10.2136/vzj2016.03.0021
- 1211 Laundré, J.W., 1989. Estimating soil bulk-density with expanding polyurethane foam. *Soil*
1212 *Sci.* 147, 223–224. doi:10.1097/00010694-198903000-00009
- 1213 Lawrence, G.P., 1978. Stability of soil pores during mercury intrusion porosimetry. *J. Soil*
1214 *Sci.* 29, 299–304.

- 1215 Le Bissonnais, Y., 1996. Aggregate stability and assessment of soil crustability and
1216 erodibility: I. Theory and methodology. *Eur. J. Soil Sci.* 47, 425–437.
1217 doi:10.1111/j.1365-2389.1996.tb01843.x
- 1218 Lehmann, P., Wyss, P., Flisch, A., Lehmann, E., Vontobel, P., Krafczyk, M., Kaestner, A.,
1219 Beckmann, F., Gygi, A., Flühler, H., 2006. Tomographical imaging and mathematical
1220 description of porous media used for the prediction of fluid distribution. *Vadose Zone J.*
1221 5, 80–97. doi:10.2136/vzj2004.0177
- 1222 Letey, J., 1991. The study of soil structure - Science or art. *Soil Res.* 29, 699–707.
1223 doi:10.1071/SR9910699
- 1224 Lowell, S., Shields, J.E., Thomas, M.A., Thommes, M., 2004. Characterization of porous
1225 solids and powders: surface area, pore size and density. Kluwer Academic Publishers,
1226 Dordrecht, The Netherlands. doi:10.1007/978-1-4020-2303-3
- 1227 Lu, Y., Liu, X., Heitman, J., Horton, R., Ren, T., 2016. Determining soil bulk density with
1228 thermo-time domain reflectometry: a thermal conductivity-based approach. *Soil Sci. Soc.*
1229 *Am. J.* 80, 48–54. doi:10.2136/sssaj2015.08.0315
- 1230 Luo, L., Lin, H., Schmidt, J., 2010. Quantitative relationships between soil macropore
1231 characteristics and preferential flow and transport. *Soil Sci. Soc. Am. J.* 74, 1929–1937.
1232 doi:10.2136/sssaj2010.0062
- 1233 Mangalassery, S., Sjögersten, S., Sparkes, D.L., Sturrock, C.J., Mooney, S.J., 2013. The effect
1234 of soil aggregate size on pore structure and its consequence on emission of greenhouse
1235 gases. *Soil Tillage Res.* 132, 39–46. doi:10.1016/j.still.2013.05.003
- 1236 Mayer, L.M., Schick, L.L., Hardy, K.R., Wagai, R., McCarthy, J., 2004. Organic matter in
1237 small mesopores in sediments and soils. *Geochim. Cosmochim. Acta* 68, 3863–3872.
1238 doi:10.1016/j.gca.2004.03.019

- 1239 McKenzie, D.C., 2001. Rapid assessment of soil compaction damage. I. The SOILpak score,
1240 a semi-quantitative measure of soil structural form. *Aust. J. Soil Res.* 39, 117–125.
1241 doi:10.1071/SR99116
- 1242 Moebius, B.N., van Es, H.M., Schindelbeck, R.R., Idowu, O.J., Clune, D.J., Thies, J.E., 2007.
1243 Evaluation of laboratory-measured soil properties as indicators of soil physical quality.
1244 *Soil Sci.* 172, 895–912. doi:10.1097/ss.0b013e318154b520
- 1245 Moni, C., Rumpel, C., Virto, I., Chabbi, A., Chenu, C., 2010. Relative importance of sorption
1246 versus aggregation for organic matter storage in subsoil horizons of two contrasting
1247 soils. *J. Soil Sci.* 61, 958–969. doi:10.1111/j.1365-2389.2010.01307.x
- 1248 Mualem, Y., 1976. A new model for predicting the hydraulic conductivity of unsaturated
1249 porous media. *Water Resour. Res.* 12, 513–522. doi:10.1029/WR012i003p00513
- 1250 Mueller, L., Kay, B.D., Hu, C., Li, Y., Schindler, U., Behrendt, A., Shepherd, T.G., Ball,
1251 B.C., 2009. Visual assessment of soil structure: evaluation of methodologies on sites in
1252 Canada, China and Germany. Part I: Comparing visual methods and linking them with
1253 soil physical data and grain yield of cereals. *Soil Tillage Res.* 103, 178–187.
1254 doi:10.1016/j.still.2008.12.015
- 1255 Munkholm, L.J., Heck, R.J., Deen, B., Zidar, T., 2016. Relationship between soil aggregate
1256 strength, shape and porosity for soils under different long-term management. *Geoderma*
1257 268, 52–59. doi:10.1016/j.geoderma.2016.01.005
- 1258 Naderi-Boldaji, M., Keller, T., 2016. Degree of soil compactness is highly correlated with the
1259 soil physical quality index S. *Soil Tillage Res.* 159, 41–46.
1260 doi:10.1016/j.still.2016.01.010
- 1261 Naveed, M., Arthur, E., De Jonge, L.W., Tuller, M., Moldrup, P., 2014a. Pore structure of
1262 natural and regenerated soil aggregates: an X-ray computed tomography analysis. *Soil*

- 1263 Sci. Soc. Am. J. 78, 377–386. doi:10.2136/sssaj2013.06.0216
- 1264 Naveed, M., Moldrup, P., Vogel, H.J., Lamandé, M., Wildenschild, D., Tuller, M., de Jonge,
1265 L.W., 2014b. Impact of long-term fertilization practice on soil structure evolution.
1266 *Geoderma* 217–218, 181–189. doi:10.1016/j.geoderma.2013.12.001
- 1267 Nciizah, A.D., Wakindiki, I.I.C., 2015. Physical indicators of soil erosion, aggregate stability
1268 and erodibility. *Arch. Agron. Soil Sci.* 61, 827–842. doi:10.1080/03650340.2014.956660
- 1269 Negassa, W.C., Guber, A.K., Kravchenko, A.N., Marsh, T.L., Hildebrandt, B., Rivers, M.L.,
1270 2015. Properties of soil pore space regulate pathways of plant residue decomposition and
1271 community structure of associated bacteria. *PLoS One* 10, 1–22.
1272 doi:10.1371/journal.pone.0123999
- 1273 Newell-Price, J.P., Whittingham, M.J., Chambers, B.J., Peel, S., 2013. Visual soil evaluation
1274 in relation to measured soil physical properties in a survey of grassland soil compaction
1275 in England and Wales. *Soil Tillage Res.* 127, 65–73. doi:10.1016/j.still.2012.03.003
- 1276 Neyshabouri, M.R., Kazemi, Z., Oustan, S., Moghaddam, M., 2014. PTFs for predicting
1277 LLWR from various soil attributes including cementing agents. *Geoderma* 226–227,
1278 179–187. doi:10.1016/j.geoderma.2014.02.008
- 1279 Nimmo, J.R., 2005. Porosity and pore size distribution, in: *Encyclopedia of Soils in the*
1280 *Environment*. Elsevier, London, pp. 295–303. doi:10.1016/B0-12-348530-4/00404-5
- 1281 Nortcliff, S., 2002. Standardisation of soil quality attributes. *Agric. Ecosyst. Environ.* 88,
1282 161–168. doi:10.1016/S0167-8809(01)00253-5
- 1283 Oades, J.M., 1984. Soil organic matter and structural stability: mechanisms and implications
1284 for management. *Plant Soil* 76, 319–337. doi:10.1007/BF02205590
- 1285 Oades, J.M., Waters, A.G., 1991. Aggregate hierarchy in soils. *Soil Res.* 29, 815–828.

- 1286 doi:10.1071/SR9910815
- 1287 Otalvaro, I.F., Neto, M.P.C., Delage, P., Caicedo, B., 2016. Relationship between soil
1288 structure and water retention properties in a residual compacted soil. *Eng. Geol.* 205, 73–
1289 80. doi:10.1016/j.enggeo.2016.02.016
- 1290 Pachepsky, Y., Rawls, W., 2003. Soil structure and pedotransfer functions. *Eur. J. Soil Sci.*
1291 54, 443–451. doi:10.1046/j.1365-2389.2003.00485.x
- 1292 Page-Dumroese, D.S., Brown, R.E., Jurgensen, M.F., Mroz, G.D., 1999. Comparison of
1293 methods for determining bulk densities of rocky forest soils. *Soil Sci. Soc. Am. J.* 63,
1294 379–383. doi:10.2136/sssaj1999.03615995006300020016x
- 1295 Pagliai, M., Vignozzi, N., 2002. The soil pore system as an indicator of soil quality. *Adv.*
1296 *GeoEcology* 35, 69–80.
- 1297 Pagliai, M., Vignozzi, N., Pellegrini, S., 2004. Soil structure and the effect of management
1298 practices. *Soil Tillage Res.* 79, 131–143. doi:10.1016/j.still.2004.07.002
- 1299 Paradelo, M., Katuwal, S., Moldrup, P., Norgaard, T., Herath, L., de Jonge, L.W., 2016. X-ray
1300 CT-derived soil characteristics explain varying air, water, and solute transport properties
1301 across a loamy field. *Vadose Zone J.* 15. doi:10.2136/vzj2015.07.0104
- 1302 Paradelo, R., van Oort, F., Chenu, C., 2013. Water-dispersible clay in bare fallow soils after
1303 80 years of continuous fertilizer addition. *Geoderma* 200–201, 40–44.
1304 doi:10.1016/j.geoderma.2013.01.014
- 1305 Paz Ferreiro, J., Miranda, J.G.V., Vidal Vázquez, E., 2010. Multifractal analysis of soil
1306 porosity based on mercury injection and nitrogen adsorption. *Vadose Zone J.* 9, 325–
1307 335. doi:10.2136/vzj2009.0090
- 1308 Peerlkamp, P.K., 1959. A visual method of soil structure evaluation. *Meded. van*

- 1309 Landbouwhoges. en der Opzoekingsstn. van den Staat te Gent 24, 216–221.
- 1310 Peng, X., Horn, R.F., Hallett, P.D., 2015. Soil structure and its functions in ecosystems: phase
1311 matter & scale matter. *Soil Tillage Res.* 146, 1–3. doi:10.1016/j.still.2014.10.017
- 1312 Pires, L.F., Bacchi, O.O.S., Reichardt, K., Timm, L.C., 2005. Application of gamma-ray
1313 computed tomography to analysis of soil structure before density evaluations. *Appl.*
1314 *Radiat. Isot.* 63, 505–11. doi:10.1016/j.apradiso.2005.03.019
- 1315 Pohlmeier, A., Oros-Peusquens, A., Javaux, M., Menzel, M.I., Vanderborght, J., Kaffanke, J.,
1316 Romanzetti, S., Lindenmair, J., Vereecken, H., Shah, N.J., 2008. Changes in soil water
1317 content resulting from *Ricinus* root uptake monitored by magnetic resonance imaging.
1318 *Vadose Zone J.* 7, 1010–1017. doi:10.2136/vzj2007.0110
- 1319 Pulido Moncada, M., Ball, B.C., Gabriels, D., Lobo, D., Cornelis, W.M., 2014a. Evaluation of
1320 soil physical quality index S for some tropical and temperate medium-textured soils. *Soil*
1321 *Sci. Soc. Am. J.* 79, 9–19. doi:10.2136/sssaj2014.06.0259
- 1322 Pulido Moncada, M., Gabriels, D., Cornelis, W., Lobo, D., 2013. Comparing aggregate
1323 stability tests for soil physical quality indicators. *L. Degrad. Dev.* 26, 843–852.
1324 doi:10.1002/ldr.2225
- 1325 Pulido Moncada, M., Gabriels, D., Lobo, D., Rey, J.C., Cornelis, W.M., 2014b. Visual field
1326 assessment of soil structural quality in tropical soils. *Soil Tillage Res.* 139, 8–18.
1327 doi:10.1016/j.still.2014.01.002
- 1328 Pulido Moncada, M., Helwig Penning, L., Timm, L.C., Gabriels, D., Cornelis, W.M., 2014c.
1329 Visual examinations and soil physical and hydraulic properties for assessing soil
1330 structural quality of soils with contrasting textures and land uses. *Soil Tillage Res.* 140,
1331 20–28. doi:10.1016/j.still.2014.02.009
- 1332 Rabbi, S.M.F., Daniel, H., Lockwood, P. V., Macdonald, C., Pereg, L., Tighe, M., Wilson,

- 1333 B.R., Young, I.M., 2016. Physical soil architectural traits are functionally linked to
1334 carbon decomposition and bacterial diversity. *Sci. Rep.* 6, 33012. doi:10.1038/srep33012
- 1335 Rabot, E., Lacoste, M., Hénault, C., Cousin, I., 2015. Using X-ray computed tomography to
1336 describe the dynamics of nitrous oxide emissions during soil drying. *Vadose Zone J.* 14.
1337 doi:10.2136/vzj2014.12.0177
- 1338 Ragab, R., Feyen, J., Hillel, D., 1982. Effect of the method for determining pore size
1339 distribution on prediction of the hydraulic conductivity function and of infiltration. *Soil*
1340 *Sci.* 134, 141–145. doi:10.1097/00010694-198208000-00009
- 1341 Ravikovitch, P.I., Bogan, B.W., Neimark, A. V., 2005. Nitrogen and carbon dioxide
1342 adsorption by soils. *Environ. Sci. Technol.* 39, 4990–4995. doi:10.1021/es048307b
- 1343 Regelink, I.C., Stoof, C.R., Rouseva, S., Weng, L., Lair, G.J., Kram, P., Nikolaidis, N.P.,
1344 Kercheva, M., Banwart, S., Comans, R.N.J., 2015. Linkages between aggregate
1345 formation, porosity and soil chemical properties. *Geoderma* 247–248, 24–37.
1346 doi:10.1016/j.geoderma.2015.01.022
- 1347 Reichert, J.M., Suzuki, L.E.A.S., Reinert, D.J., Horn, R., Håkansson, I., 2009. Reference bulk
1348 density and critical degree-of-compactness for no-till crop production in subtropical
1349 highly weathered soils. *Soil Tillage Res.* 102, 242–254. doi:10.1016/j.still.2008.07.002
- 1350 Reinhart, K.O., Nichols, K.A., Petersen, M., Vermeire, L.T., 2015. Soil aggregate stability
1351 was an uncertain predictor of ecosystem functioning in a temperate and semiarid
1352 grassland. *Ecosphere* 6, 1–16. doi:10.1890/ES15-00056.1
- 1353 Renard, P., Allard, D., 2013. Connectivity metrics for subsurface flow and transport. *Adv.*
1354 *Water Resour.* 51, 168–196. doi:10.1016/j.advwatres.2011.12.001
- 1355 Renger, M., 1970. Über den Einfluss der Dränung auf das Gefüge und die
1356 Wasserdurchlässigkeit bindiger Böden. *Mitteilungen der Dtsch. Bodenkundlichen*

- 1357 Gesellschaft 11, 23–28.
- 1358 Renger, M., Bohne, K., Facklam, M., Harrach, T., Riek, W., Schäfer, W., Wessolek, G.,
1359 Zacharias, S., 2008. Ergebnisse und Vorschläge der DGB-Arbeitsgruppe “Kennwerte des
1360 Bodgengefüges” zur Schätzung bodenphysikalischer Kennwerte. Berlin.
- 1361 Reynolds, W.D., Drury, C.F., Tan, C.S., Fox, C.A., Yang, X.M., 2009. Use of indicators and
1362 pore volume-function characteristics to quantify soil physical quality. *Geoderma* 152,
1363 252–263. doi:10.1016/j.geoderma.2009.06.009
- 1364 Richard, G., Cousin, I., Sillon, J.F., Bruand, A., Guéris, J., 2001. Effect of compaction on soil
1365 porosity: consequences on hydraulic properties. *Eur. J. Soil Sci.* 52, 49–58.
1366 doi:10.1046/j.1365-2389.2001.00357.x
- 1367 Roger-Estrade, J., Richard, G., Boizard, H., Boiffin, J., Caneill, J., Manichon, H., 2000.
1368 Modelling structural changes in tilled topsoil over time as a function of cropping
1369 systems. *Eur. J. Soil Sci.* 51, 455–474. doi:10.1046/j.1365-2389.2000.00323.x
- 1370 Roger-Estrade, J., Richard, G., Caneill, J., Boizard, H., Coquet, Y., Defosse, P., Manichon,
1371 H., 2004. Morphological characterisation of soil structure in tilled fields: from a
1372 diagnosis method to the modelling of structural changes over time. *Soil Tillage Res.* 79,
1373 33–49. doi:10.1016/j.still.2004.03.009
- 1374 Roger-Estrade, J., Richard, G., Dexter, A.R., Boizard, H., de Tourdonnet, S., Bertrand, M.,
1375 Caneill, J., 2009. Integration of soil structure variations with time and space into models
1376 for crop management. A review. *Agron. Sustain. Dev.* 29, 135–142.
1377 doi:10.1051/agro:2008052
- 1378 Romero, E., Simms, P.H., 2008. Microstructure investigation in unsaturated soils: a review
1379 with special attention to contribution of mercury intrusion porosimetry and
1380 environmental scanning electron microscopy. *Geotech. Geol. Eng.* 26, 705–727.

1381 doi:10.1007/s10706-008-9204-5

1382 Rossi, A.M., Hirmas, D.R., Graham, R.C., Sternberg, P.D., 2008. Bulk density determination
1383 by automated three-dimensional laser scanning. *Soil Sci. Soc. Am. J.* 72, 1591–1593.
1384 doi:10.2136/sssaj2008.0072N

1385 Ruamps, L.S., Nunan, N., Chenu, C., 2011. Microbial biogeography at the soil pore scale.
1386 *Soil Biol. Biochem.* 43, 280–286. doi:10.1016/j.soilbio.2010.10.010

1387 Rücknagel, J., Hofmann, B., Paul, R., Christen, O., Hülsbergen, K.J., 2007. Estimating
1388 precompression stress of structured soils on the basis of aggregate density and dry bulk
1389 density. *Soil Tillage Res.* 92, 213–220. doi:10.1016/j.still.2006.03.004

1390 Sandin, M., Koestel, J., Jarvis, N., Larsbo, M., 2017. Post-tillage evolution of structural pore
1391 space and saturated and near-saturated hydraulic conductivity in a clay loam soil. *Soil*
1392 *Tillage Res.* 165, 161–168. doi:10.1016/j.still.2016.08.004

1393 Schaap, J.D., Lehmann, P., Kaestner, A., Vontobel, P., Hassanein, R., Frei, G., de Rooij,
1394 G.H., Lehmann, E., Flühler, H., 2008. Measuring the effect of structural connectivity on
1395 the water dynamics in heterogeneous porous media using speedy neutron tomography.
1396 *Adv. Water Resour.* 31, 1233–1241. doi:10.1016/j.advwatres.2008.04.014

1397 Schlüter, S., Sheppard, A., Brown, K., Wildenschild, D., 2014. Image processing of
1398 multiphase images obtained via X-ray microtomography: a review. *Water Resour. Res.*
1399 50, 3615–3639. doi:10.1002/2014WR015256

1400 Schlüter, S., Vogel, H.J., 2016. Analysis of soil structure turnover with garnet particles and X-
1401 ray microtomography. *PLoS One* 11, e0159948. doi:10.1371/journal.pone.0159948

1402 Schlüter, S., Weller, U., Vogel, H.J., 2011. Soil-structure development including seasonal
1403 dynamics in a long-term fertilization experiment. *J. Plant Nutr. Soil Sci.* 174, 395–403.
1404 doi:10.1002/jpln.201000103

1405 Schoeneberger, P.J., Wysocki, D.A., Benham, E.C., Soil Survey Staff, 2012. Field book for
1406 describing and sampling soils, v. 3.0. Natural Resources Conservation Service, National
1407 Soil Survey Center, Lincoln, NE.

1408 Séquaris, J.M., Guisado, G., Magarinos, M., Moreno, C., Burauel, P., Narres, H.D.,
1409 Vereecken, H., 2010. Organic-carbon fractions in an agricultural topsoil assessed by the
1410 determination of the soil mineral surface area. *J. Plant Nutr. Soil Sci.* 173, 699–705.
1411 doi:10.1002/jpln.200800224

1412 Seybold, C.A., Mausbach, M.J., Karlen, D.L., Rogers, H.H., 1998. Quantification of soil
1413 quality, in: Lal, R., Kimble, J.M., Follet, R.F., Stewart, B.A. (Eds.), *Soil Processes and
1414 the Carbon Cycle*. CRC Press LLC, Boca Raton, FL, pp. 387–404.

1415 Shepherd, T.G., 2009. Visual soil assessment. Volume 1. Field guide for pastoral grazing and
1416 cropping on flat to rolling country, 2nd ed. Horizons Regional Council, Palmerston
1417 North.

1418 Shepherd, T.G., 2003. Assessing soil quality using visual soil assessment, in: Currie, L.D.,
1419 Hanly, J.A. (Eds.), *Tools for Nutrient and Pollutant Management: Applications to
1420 Agriculture and Environmental Quality*. Fertilizer and Lime Research Centre, Massey
1421 University, Palmerston North, pp. 153–166.

1422 Shepherd, T.G., 2000. Visual Soil Assessment. Volume 1. Field guide for cropping and
1423 pastoral grazing on flat to rolling country. horizons.mw & Landcare Research,
1424 Palmerston North.

1425 Shepherd, T.G., Stagnari, F., Pisante, M., Benites, J., 2008. Visual soil assessment - Field
1426 guide for annual crops. Rome, Italy.

1427 Simms, P.H., Yanful, E.K., 2001. Measurement and estimation of pore shrinkage and pore
1428 distribution in a clayey till during soil-water characteristic curve tests. *Can. Geotech. J.*

1429 38, 741–754. doi:10.1139/t01-014

1430 Sing, K.S.W., Everett, D.H., Haul, R.A.W., Moscou, L., Pierotti, R.A., Rouquerol, J.,
1431 Siemieniewska, T., 2008. Reporting physisorption data for gas/solid systems, in:
1432 Handbook of Heterogeneous Catalysis. Wiley-VCH Verlag GmbH & Co. KGaA, pp.
1433 1217–1230. doi:10.1002/9783527610044.hetcat0065

1434 Six, J., Bossuyt, H., Degryze, S., Denef, K., 2004. A history of research on the link between
1435 (micro)aggregates, soil biota, and soil organic matter dynamics. *Soil Tillage Res.* 79, 7–
1436 31. doi:10.1016/j.still.2004.03.008

1437 Six, J., Conant, R.T., Paul, E.A., Paustian, K., 2002. Stabilization mechanisms of soil organic
1438 matter: implications for C-saturation of soils. *Plant Soil* 241, 155–176.
1439 doi:10.1023/A:1016125726789

1440 Six, J., Paustian, K., 2014. Aggregate-associated soil organic matter as an ecosystem property
1441 and a measurement tool. *Soil Biol. Biochem.* 68, A4–A9.
1442 doi:10.1016/j.soilbio.2013.06.014

1443 Skvortsova, E.B., Sanzharova, S.I., 2007. Micromorphometric features of pore space in the
1444 plow horizons of loamy soils. *Eurasian Soil Sci.* 40, 445–455.
1445 doi:10.1134/S1064229307040114

1446 Skvortsova, E.B., Utkaeva, V.F., 2008. Soil pore space arrangement as a geometric indicator
1447 of soil structure. *Eurasian Soil Sci.* 41, 1198–1204. doi:10.1134/S1064229308110082

1448 Sněhota, M., Císlarová, M., Amin, M.H.G., Hall, L.D., 2010. Tracing the entrapped air in
1449 heterogeneous soil by means of magnetic resonance imaging. *Vadose Zone J.* 9, 373–
1450 384. doi:10.2136/vzj2009.0103

1451 Soil Survey Staff, 2014. Soil survey field and laboratory methods manual. Soil survey
1452 investigations, report No. 51, v.2. U.S. Department of Agriculture, Natural Resources

1453 Conservation Service.

1454 Strong, D.T., De Wever, H., Merckx, R., Recous, S., 2004. Spatial location of carbon
1455 decomposition in the soil pore system. *Eur. J. Soil Sci.* 55, 739–750. doi:10.1111/j.1365-
1456 2389.2004.00639.x

1457 Thompson, M.L., McBride, J.F., Horton, R., 1985. Effects of drying treatments on porosity of
1458 soil materials. *Soil Sci. Soc. Am. J.* 49, 1360–1364.
1459 doi:10.2136/sssaj1985.03615995004900060006x

1460 Throop, H.L., Archer, S.R., Monger, H.C., Waltman, S., 2012. When bulk density methods
1461 matter: implications for estimating soil organic carbon pools in rocky soils. *J. Arid
1462 Environ.* 77, 66–71. doi:10.1016/j.jaridenv.2011.08.020

1463 Timm, L.C., Pires, L.F., Reichardt, K., Roveratti, R., Oliveira, J.C.M., Bacchi, O.O.S., 2005.
1464 Soil bulk density evaluation by conventional and nuclear methods. *Aust. J. Soil Res.* 43,
1465 97–103. doi:10.1071/SR04054

1466 Tisdall, J.M., Oades, J.M., 1982. Organic matter and water-stable aggregates in soils. *J. Soil
1467 Sci.* 33, 141–163. doi:10.1111/j.1365-2389.1982.tb01755.x

1468 Toosi, E.R., Kravchenko, A.N., Mao, J., Quigley, M.Y., Rivers, M.L., 2017. Effects of
1469 management and pore characteristics on organic matter composition of macroaggregates:
1470 evidence from characterization of organic matter and imaging. *Eur. J. Soil Sci.* 68, 200–
1471 211. doi:10.1111/ejss.12411

1472 Tuller, M., Kulkarni, R., Fink, W., 2013. Segmentation of X-ray CT data of porous materials:
1473 a review of global and locally adaptive algorithms, in: Anderson, S.H., Hopmans, J.W.
1474 (Eds.), *Soil–Water–Root Processes: Advances in Tomography and Imaging*, SSSA
1475 Special Publication 61. The Soil Science Society of America, Inc., Madison, WI, pp.
1476 157–182. doi:10.2136/sssaspecpub61.c8

- 1477 Tumlinson, L.G., Liu, H., Silk, W.K., Hopmans, J.W., 2008. Thermal neutron computed
1478 tomography of soil water and plant roots. *Soil Sci. Soc. Am. J.* 72, 1234–1242.
1479 doi:10.2136/sssaj2007.0302
- 1480 Uteau, D., Pagenkemper, S.K., Peth, S., Horn, R., 2013. Aggregate and soil clod volume
1481 measurement: a method comparison. *Soil Sci. Soc. Am. J.* 77, 60–63.
1482 doi:10.2136/sssaj2012.0227n
- 1483 Van Brakel, J., Modrý, S., Svatá, M., 1981. Mercury porosimetry: state of the art. *Powder*
1484 *Technol.* 29, 1–12. doi:10.1016/0032-5910(81)85001-2
- 1485 van Genuchten, M.T., 1980. A closed-form equation for predicting the hydraulic conductivity
1486 of unsaturated soils. *Soil Sci. Soc. Am. J.* 44, 892–898.
1487 doi:10.2136/sssaj1980.03615995004400050002x
- 1488 Vereecken, H., Weynants, M., Javaux, M., Pachepsky, Y., Schaap, M.G., Van Genuchten,
1489 M.T., 2010. Using pedotransfer functions to estimate the van Genuchten–Mualem soil
1490 hydraulic properties: a review. *Vadose Zone J.* 9, 795–820. doi:10.2136/vzj2010.0045
- 1491 Vincent, K.R., Chadwick, O.A., 1994. Synthesizing bulk density for soils with abundant rock
1492 fragments. *Soil Sci. Soc. Am. J.* 58, 455–464.
1493 doi:10.2136/sssaj1994.03615995005800020030x
- 1494 Virto, I., Barré, P., Chenu, C., 2008. Microaggregation and organic matter storage at the silt-
1495 size scale. *Geoderma* 146, 326–335. doi:10.1016/j.geoderma.2008.05.021
- 1496 Vogel, H.J., 2000. A numerical experiment on pore size, pore connectivity, water retention,
1497 permeability, and solute transport using network models. *Eur. J. Soil Sci.* 51, 99–105.
1498 doi:10.1046/j.1365-2389.2000.00275.x
- 1499 Vogel, H.J., Cousin, I., Roth, K., 2002. Quantification of pore structure and gas diffusion as a
1500 function of scale. *Eur. J. Soil Sci.* 53, 465–473. doi:10.1046/j.1365-2389.2002.00457.x

- 1501 Vogel, H.J., Weller, U., Schlüter, S., 2010. Quantification of soil structure based on
1502 Minkowski functions. *Comput. Geosci.* 36, 1236–1245. doi:10.1016/j.cageo.2010.03.007
- 1503 Wallace, K.J., 2007. Classification of ecosystem services: Problems and solutions. *Biol.*
1504 *Conserv.* 139, 235–246. doi:10.1016/j.biocon.2007.07.015
- 1505 Wildenschild, D., Hopmans, J.W., Vaz, C.M.P., Rivers, M.L., Rikard, D., Christensen,
1506 B.S.B., 2002. Using X-ray computed tomography in hydrology: systems, resolutions,
1507 and limitations. *J. Hydrol.* 267, 285–297. doi:10.1016/S0022-1694(02)00157-9
- 1508 Wildenschild, D., Sheppard, A.P., 2013. X-ray imaging and analysis techniques for
1509 quantifying pore-scale structure and processes in subsurface porous medium systems.
1510 *Adv. Water Resour.* 51, 217–246. doi:10.1016/j.advwatres.2012.07.018
- 1511 Young, I.M., Crawford, J.W., Nunan, N., Otten, W., Spiers, A., 2008. Microbial distribution
1512 in soils: physics and scaling, in: Sparks, D.L. (Ed.), *Advances in Agronomy*. Academic
1513 Press, Burlington, pp. 81–121. doi:10.1016/S0065-2113(08)00604-4
- 1514 Young, I.M., Crawford, J.W., Rappoldt, C., 2001. New methods and models for
1515 characterising structural heterogeneity of soil. *Soil Tillage Res.* 61, 33–45.
1516 doi:10.1016/S0167-1987(01)00188-X
- 1517 Zachara, J., Brantley, S., Chorover, J., Ewing, R., Kerisit, S., Liu, C., Perfect, E., Rother, G.,
1518 Stack, A., 2016. Internal domains of natural porous media revealed: critical locations for
1519 transport, storage, and chemical reaction. *Environ. Sci. Technol.* 50, 2811–2829.
1520 doi:10.1021/acs.est.5b05015
- 1521 Zacharias, S., Bohne, K., 2008. Attempt of a flux-based evaluation of field capacity. *J. Plant*
1522 *Nutr. Soil Sci.* 171, 399–408. doi:10.1002/jpln.200625168
- 1523 Zong, Y., Yu, X., Zhu, M., Lu, S., 2015. Characterizing soil pore structure using nitrogen
1524 adsorption, mercury intrusion porosimetry, and synchrotron-radiation-based X-ray

1525 computed microtomography techniques. *J. Soils Sediments* 15, 302–312.

1526 doi:10.1007/s11368-014-0995-0

1527

Figure captions

Figure 1: Sketch of a structural map for the evaluation of the percentage of Δ clod surface (black). Reprinted from Roger-Estrade et al. (2004), with permission from Elsevier.

Figure 2: Visual key for scoring soil structure after a drop-shatter test. (a) Good, (b) moderate, and (c) poor physical condition. Reprinted from Shepherd et al. (2008).

Figure 3: Comparison of the sample sizes and pore sizes investigated with the different methods to characterize soil pore space. Both axes are represented with a logarithmic scale.

Figure 4: Indicators derived from the water retention curve.

Figure 5: Least limiting water range (LLWR) of a loamy soil as function of bulk density. The left arrow represents the LLWR at the bulk density of 1.1 g cm^{-3} , where plant growth is limited by field capacity and permanent wilting point. The right arrow represents the LLWR at the bulk density of 1.4 g cm^{-3} , where high penetration resistance and low air capacity further reduce the LLWR. Redrawn from Kaufmann et al. (2010).

Figure 6: Summary of two competing views: the aggregate perspective and the pore space perspective. (a) Kühnfeld, Halle, Germany (continuous maize, conventional tillage, 63% sand, 25% silt, 12% clay), (b) Hadera, Israel (orchard, 65% sand, 16% silt, 19% clay), (c) Bad Lauchstädt, Germany (grassland, 12% sand, 68% silt, 20% clay), (d) Garzweiler, Germany (crop rotation, below plow layer, 5% sand, 81% silt, 14% clay).

Tables

Table 1: Comparison of different measurement methods and indicators of soil structure.

Measurement method	Indicator	Sample size	Pore size observed	Level of expertise ^a	Reproducibility ^b	Duration ^c	Cost	Measure	Methodological limitations
Whole profile evaluation	Grade, size, shape of peds	Horizon	> 200 μm	High	Medium	Half an hour + pit	Low	Qualitative	- Subjective - Depends on soil texture and moisture
	% Δ clod surface	Profile of a few meters length, 1-m depth	> 200 μm	High	Medium	A few hours + pit	Low	Quantitative	
Topsoil evaluation	Visual evaluation score	Full size of a spade and \approx 20 cm-thick	> 200 μm	Medium	Medium	Half an hour	Low	Semi-quantitative	- Subjective - Depends on soil texture, moisture, and biological activity - Difficulty in breaking soil manually along planes of weakness - Compaction may occur during the drop-shatter test or by breaking soil manually
Bulk density	Bulk density	Hundreds cm^3 to hundreds dm^3	-	Low	High	Half an hour + drying	Low	Quantitative	- Difficulties with soils with abundant rock fragments, plant roots, or residues - Depends on soil moisture - Compaction may occur with the core method - Inadequate representation of large pores with the clod method - No standard method to evaluate the reference BD - Not satisfying for organic soils, doubt for sandy soils - (Poorly explored so far)
				Medium	Medium	A few hours + drying	Medium		
	Low	High	A few hours + drying	Low					
Aggregate size distribution and stability	Stability index	Tens to hundred g	-	Medium	Low	A few hours	Low	Quantitative	- Wide number of measurement methods - Unknown applied energy - Non-negligible effect of the type of sieving, duration, oscillation frequency, loading rate, number and size of sieves, storage duration, and pretreatment (moisture history)
	Aggregate size distribution Water-dispersible clay Microaggregates-within-macroaggregates								
Mercury porosimetry	Porosity	A few cm^3	0.003 to 500 μm	Low	High	A few hours	Medium	Quantitative	- Assumes non-connected cylindrical pores - Ink-bottle effect - Contact angle of mercury with soil surface often unknown - Sample dried
	Macroporosity Microporosity								

Water retention curve	Porosity Macroporosity Microporosity Air capacity Relative field capacity Available water capacity LLWR S index	Hundreds cm ³ to dm ³	0.2 to 3000 μm	Medium	High	Days to weeks	Medium	Quantitative	- Assumes non-connected cylindrical pores - Ink-bottle effect - Adjustment of a model can introduce small errors
Gas adsorption	Specific surface area Mesoporosity (2–50 nm) Microporosity (< 2 nm)	1 to tens mm ³	0.001 to 0.2 μm	High	Medium	A few hours to days	Medium	Quantitative	- Assumes an idealized pore shape - Sample dried - N ₂ inadequate to characterize soils with high amounts of SOM
Imaging techniques (lab)	Porosity Macroporosity Microporosity Connectivity Pore orientation Pore shape	1 cm ³ to dm ³	A few μm to hundreds μm	High	Medium	A few hours	High	Quantitative	- Sensitive to the segmentation step and image resolution

^a High: several protocols exist to perform the measurement and/or to analyze the data, which need to be adapted for the case study, a dedicated training and experience is required; Medium: several protocols exist to perform the measurement and/or to analyze the data, which need to be adapted for the case study, but skills can be learned easily; Low: a protocol exist to perform the measurement and/or to analyze the data, skills can be learned easily.

^b Different operators characterize the same soil sample and choose between the different protocols available to perform the measurement and/or to analyze the data. The step of soil sampling is not taken into account. High: same results; Medium: same results to same trends; Low: same results to different trends.

^c We aimed at showing how labor-intensive the methods are for a single sample. The step of soil sampling is not taken into account.

Table 2: Comparison of indicators of soil structure to assess soil functions.

Measurement method	Indicator	Soil function					
		Biomass production	Storage and filtering of water	Storage and recycling of nutrients	Carbon storage	Habitat for biological activity	Physical stability and support
Whole profile evaluation	Ped grade		×				
	Ped size						
	Ped shape						
	% Δ clod surface		×				×
Topsoil evaluation	Visual evaluation score	×	×				×
Bulk density	Bulk density	(×)					×
	Degree of compactness	×	×				
	Packing density	×					
Aggregate size distribution and stability	Stability index		×	×			×
	Aggregate size distribution	×	×		×		×
	Water-dispersible clay		×	×			×
	Microaggregates-within-macroaggregates				×		
Mercury porosimetry	Porosity						
	Macroporosity					×	(×)
	Microporosity					×	
Water retention curve	Porosity		×				
	Macroporosity	×				×	
	Microporosity					×	
	Air capacity	×					
	Relative field capacity	×		×		×	
	Available water capacity	×	×				
	LLWR	(×)					
S index	(×)	×				×	
Gas adsorption	Specific surface area				(×)		
	Mesoporosity (2–50 nm)						
	Microporosity (< 2 nm)						
Imaging techniques	Porosity	×	×	(×)			×
	Macroporosity	×	×	(×)	×	×	
	Microporosity	×	×	(×)	×	×	
	Connectivity		×	(×)	×		×
	Pore orientation		×	(×)			
	Pore shape		×	(×)			

Figures

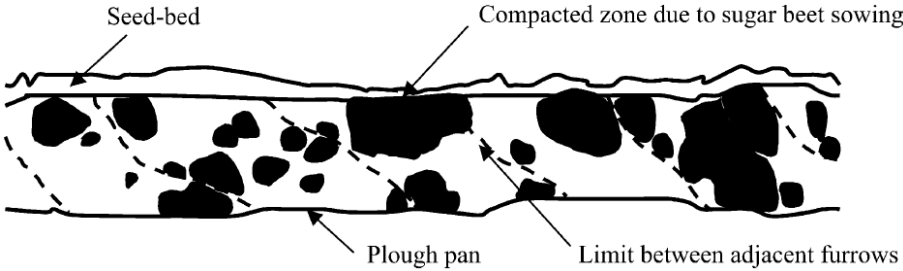


Figure 1: Sketch of a structural map for the evaluation of the percentage of Δ clod surface (black). Reprinted from Roger-Estrade et al. (2004), with permission from Elsevier.



Figure 2: Visual key for scoring soil structure after a drop-shatter test. (a) Good, (b) moderate, and (c) poor physical condition. Reprinted from Shepherd et al. (2008).

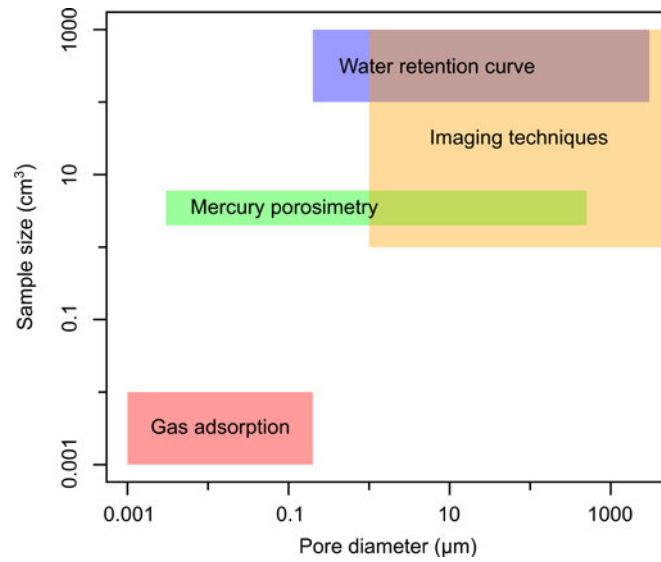


Figure 3: Comparison of the sample sizes and pore sizes investigated with the different methods to characterize soil pore space. Both axes are represented with a logarithmic scale.

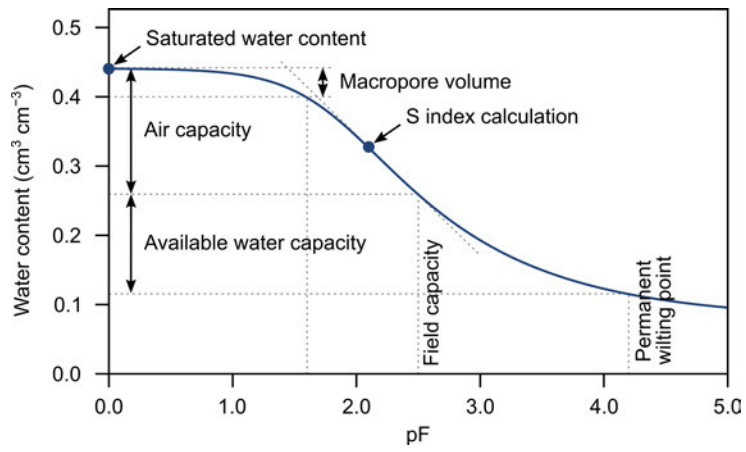


Figure 4: Indicators derived from the water retention curve.

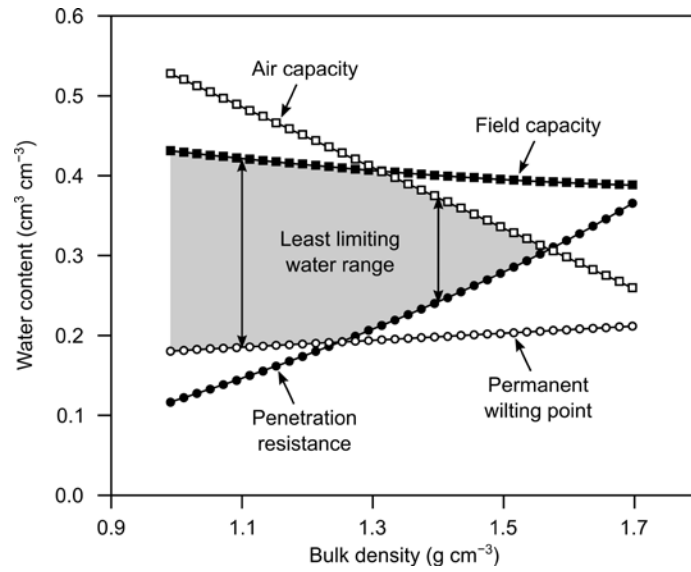


Figure 5: Least limiting water range (LLWR) of a loamy soil as function of bulk density. The left arrow represents the LLWR at the bulk density of 1.1 g cm^{-3} , where plant growth is limited by field capacity and permanent wilting point. The right arrow represents the LLWR at the bulk density of 1.4 g cm^{-3} , where high penetration resistance and low air capacity further reduce the LLWR. Redrawn from Kaufmann et al. (2010).

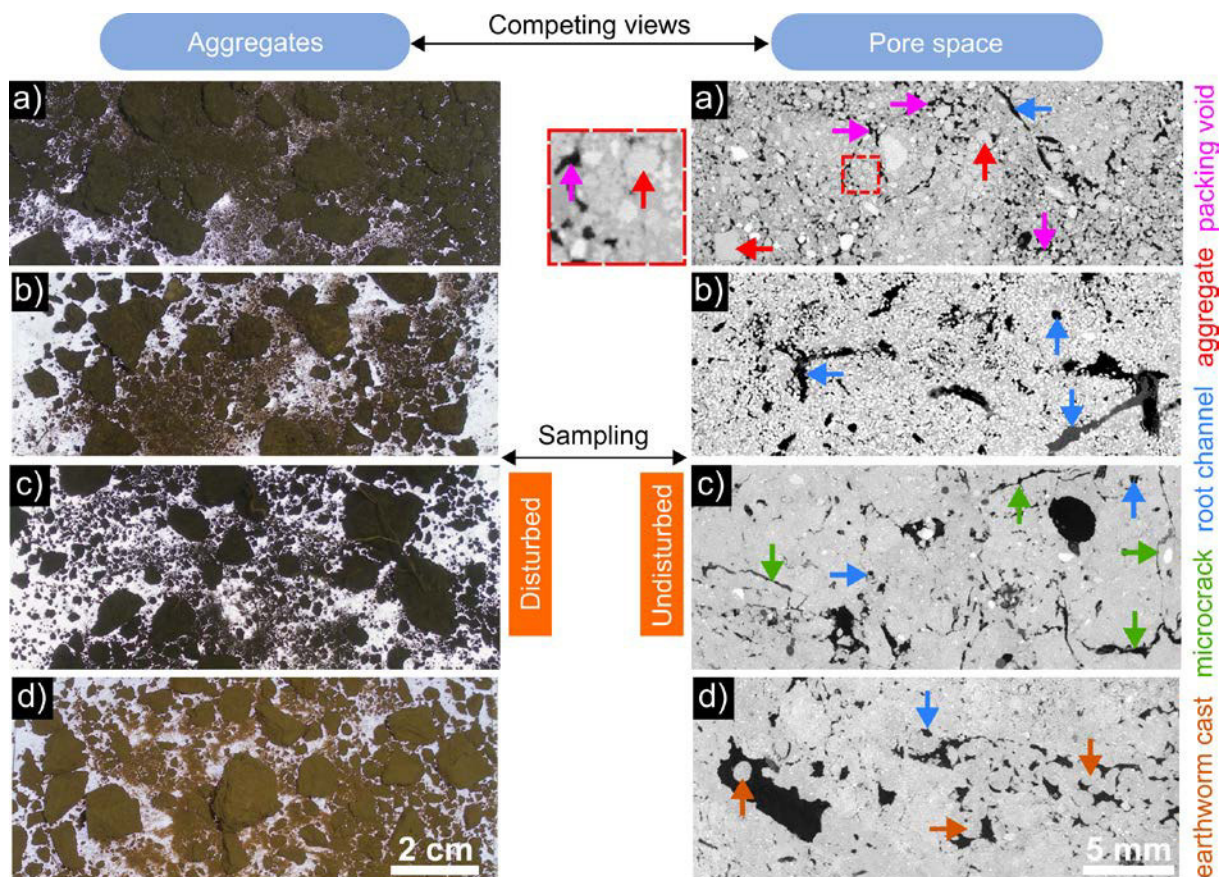


Figure 6: Summary of two competing views: the aggregate perspective and the pore space perspective. (a) Kühnfeld, Halle, Germany (continuous maize, conventional tillage, topsoil, 63% sand, 25% silt, 12% clay), (b) Hadera, Israel (orchard, topsoil, 65% sand, 16% silt, 19% clay), (c) Bad Lauchstädt, Germany (grassland, topsoil, 12% sand, 68% silt, 20% clay), (d) Garzweiler, Germany (crop rotation, below plow layer, 5% sand, 81% silt, 14% clay).